ARTICLE

Coupling of RAFT Polymerization and Chemoselective Post-modifications of Elastin-like Polypeptides for the Synthesis of Gene Delivery Vectors

Received 10th September 2020,
Accepted 18th November 2020

DOI: 10.1039/D0PY01293A

Lourdes Mónica Bravo-Anaya,*[a] Julien Rosselgong,*[a] Karla Gricelda Fernández-Solís,[a,b] Ye Xiao,[a] Amélie Vax,[a] Emmanuel Ibarboure,[a] Anna Ruban,[a] Coralie Lebleu,[a] Gilles Joucla,[c] Bertrand Garbay,[a] Elisabeth Garanger [a] and Sébastien Lecommandoux [a]

Hybrids of synthetic polymers and biopolymers are known to be macromolecular systems that merge the properties of each component and overcome some of their intrinsic limitations. Elastin-like polypeptides (ELPs) are a class of biopolymers known for their genetically-encoded synthesis, monodispersity, biocompatibility and absence of toxicity, which are very attractive features for biological applications. However, the presence of numerous amino acid residues presenting electrically charged side chains within the ELP sequence makes the purification of these ELPs by *Inverse Transition Cycling* (ITC) difficult to achieve. Positively charged ELPs are of great interest for the design of polyelectrolyte complexes dedicated to the transport and delivery of genetic material. In this work, an ELP containing periodically spaced methionine residues was recombinantly expressed, and these residues were chemoselectively modified at the thioether side chains to introduce alkyne groups. In parallel, four cationic oligomers with different chain lengths were synthesized by Reversible Addition-Fragmentation chain Transfer (RAFT) polymerization using a chain transfer agent containing an azido group. Hybrid cationic ELP were finally obtained by covalent coupling of the cationic oligomers onto the ELP by Huisgen azide-alkyne cycloaddition reaction. The different hybrid cationic ELPs were characterized by ^{1}H NMR, ζ-potential and SEC analyses to assess their purity and determine their degree of functionalization, overall charge and molar mass. Then, electrostatic complexation was achieved between these hybrid cationic ELPs and plasmid DNA, allowing the determination of the optimal conditions for obtaining stable nanoparticles having a controlled size and surface potentials at different N^+/P^- charge ratios. Preliminary biological tests showed the reliability of such hybrid cationic ELPs to internalize efficiently genetic material into living cells.

A. Introduction

Since the middle of the 20th century, synthetic polymers and their hybrids with biological molecules have been increasingly used in biotechnology, biomedical and pharmaceutical technologies.[1,2] While the design requirements can vary widely according to the application, the molar mass, (supra)molecular architecture, composition and chemical functionality appear to be the most important properties for a wide variety of applications, ranging from semi-conductor manufacturing,[3] anti-fouling surfaces,[4] polymeric drug delivery systems[5,6] or gene delivery applications.[7,8]

[a.] *University of Bordeaux, CNRS, Bordeaux INP, LCPO, UMR 5629, F-33600, Pessac, France*
[b.] *Centro Universitario UTEG, Departamento de Investigación, Héroes Ferrocarrileros #1325 C.P. 44460, Guadalajara, Jalisco, México.*
[c.] *University of Bordeaux, CNRS, Bordeaux INP, CBMN, UMR 5248, F-33615, Pessac, France.*

Electronic Supplementary Information (ESI) available: Experimental and synthetic procedures, ^{1}H NMR spectra, SEC traces, IR and ζ-potential measurements, processing procedure of the cytometry assays, cell movie and additional TEM images are available in the supporting information. See DOI: 10.1039/D0PY01293A

Biohybrid polymers are made of synthetic macromolecules with natural ones such as polysaccharides, nucleic acids, peptides and proteins.[9] This kind of materials offers the opportunity to merge the precision and versatility of polymer chemistry with the physicochemical and biological properties of biomacromolecules.[10-12] Polysaccharide graft copolymers and glycopolymers have been widely studied and used in various applications.[13] Polysaccharide block copolymers can bring an added value such as the biodegradability, the biocompatibility or the bioactivity in many cases. Some examples of polysaccharide graft copolymers with self-assembly properties have been studied for their different potential applications as biomaterials or as controlled release systems.[13] The two main approaches for the synthesis of polysaccharide graft copolymers are the polymerization of a synthetic monomer from the reactive functions of the polysaccharide backbone, and the grafting of a preformed synthetic polymer chains on the same reactive groups.[13-15] The combination of synthetic polymers and DNA has also provided scientists with new hybrid materials presenting morphologies and functions that can be controlled by the nature of the synthetic polymer segment, and by the sequence composition and length of DNA.[16] DNA and synthetic polymers can be associated to enhance profitable chemical and biological behaviors, and to reduce or suppress undesirable properties. One interesting recent example consists of linear amphiphilic DNA block copolymers (DBCs), which are able to form nanoparticles with a shell composed by DNA chains and a core of hydrophobic polymer, through microphase separation. It has been shown by Alemdaroglu *et al.* that DBC nanoparticles size can be controlled by enzymatic reactions of a non-template-dependent DNA polymerase.[17] The progress in both peptide and polymer chemistry has also led to the preparation of hybrids materials presenting properties that would not be achievable with each separate component.[18] The work of Klok *et al.* is an example of the synthesis and study of solid-state/melt properties of block copolymers composed by PEG and an amphiphilic b strand peptide.[19] Then, van Hest *et al.* proposed a combination of protein engineering and bio-conjugation for the preparation of triblock copolymers consisting of a central β-sheet polypeptide block composed of the repetitive $[(AG)_3EG]_n$ sequence conjugated to poly(ethylene glycol) (PEG) end blocks.[20] Different techniques are now available for the synthesis of polymer architectures having (poly)peptides in the main chain and in the side chain.[21] As an example, oligopeptides modified with a monomer or initiator moieties can be introduced in polymers through controlled (radical) polymerization methods. Furthermore, ligation methods allow the construction of large peptide structures through an organic chemistry approach.[21]

Recently, precision recombinant polymers were developed through recombinant protein-engineering techniques. Among them, recombinant elastin-like polypeptides (ELPs) are a special class of precision protein-like polymers with stimuli-responsive self-assembly properties, mainly developed for their potential use in biomedical applications.[22-24] ELPs are composed of repeating pentapeptide sequences -Val-Pro-Gly-*Xaa*-Gly-, (-VPGXG-), where the guest residue (*Xaa*, X) can be the combination of any amino acid except proline (Pro, P).[25-27] ELPs with accurately controlled sequences and molar masses can be produced by protein engineering techniques. These biopolymers undergo a reversible phase transition, which can be triggered by different environmental stimuli, such as ionic strength, temperature and pH.[27-29] ELPs are soluble in aqueous media at low temperatures, and phase separate as aggregates at a temperature called the inverse transition temperature (T_t), also referred to as lower critical solution temperature (LCST).[24,30,31] The T_t can be tuned by modifying ELP macromolecular parameters, *i.e.* the molar mass and the nature of the guest residue in the polypeptide sequence, and also by adjusting the ELP concentration.[24,32-34] In contrast with many synthetic polymers, ELPs are also constituted of natural amino acids that can be degraded into non-toxic metabolites.[35] Actually, the field of ELPs applications has been growing in diverse technologies due to the possible tuning of their physicochemical properties and addition of biological functions. Therefore, different ELP sequences have been conjugated to small organic molecules,[36] drugs,[37-39] oligonucleotides,[40] and polysaccharides.[41]

The development of hybrid protein–polymer bioconjugates includes nowadays ELPs as protein blocks. Le Fer *et al.* recently reported the synthesis of polymer-ELP conjugates, combining the advantages of ELPs and synthetic polypeptides to obtain "hybrid" amphiphilic diblock recombinant/synthetic polypeptides, *i.e.* Poly(γ-benzyl-L-glutamate)-*block*-ELP, capable of self-assembling in different biocompatible nano-structures.[42] Ayres *et al.* worked on the synthesis of ABA triblock copolymers, containing elastin oligopeptides as A blocks, using atom transfer radical polymerization (ATRP). These triblock copolymers were prepared by polymerizing a VPGVG monomer with a bifunctional (PEG)-based initiator.[43,44] Furthermore, ROMP-derived elastin-based oligomers were prepared from decapeptide monomers and were characterized for their thermally responsive behaviors. From these studies, it was demonstrated that ROMP could be performed on monomers bearing more than six amino acid residues (10 residues) even in the presence of sterically bulky groups and several amides.[45,46] Gao *et al.* reported the *in situ* growth of a thermoresponsive dumbbell-like polymer conjugate of a genetically engineered triblock elastin-like polypeptide (tELP).[47] They used ATRP to directly grow a PEG-like polymer selectively from the first and third blocks of the tELP to form a poly(oligo(ethylene glycol) methyl ether methacrylate) (poly(OEGMA)) brush conjugate. Moreover, elastin-based side-chain polymers (EBPs) were synthesized through the polymerization of a methacrylate derivative of the pentapeptide valine-proline-glycine-valine-glycine (VPGVG) using reversible addition-fragmentation chain transfer (RAFT) polymerization.[48] Since RAFT technique allows the introduction of functional groups such as thiols at the polymer chain end, it was proposed that EBPs prepared by RAFT could be used as mimics of ELPs for applications such as protein purification or drug delivery.[48,49] Weller *et al.* synthesized high molar mass cylindrical brush polymers with polypeptide side chains by polymerization of their respective macro-monomers, confirming that polymerization in the concentrated phase of a phase separated solution allows obtaining high degrees of main chain polymerization.[50]

As seen from the previously mentioned polymerization techniques, the arising of reversible deactivation radical polymerization (RDRP) techniques[51] such as ATRP[52,53] and reversible addition–fragmentation chain transfer polymerization (RAFT)[54] have revolutionized modern polymer science during the past two decades.[55] Though, among these techniques, RAFT allows an excellent control of polymerization over a wide variety of radically polymerizable monomers. In addition, RAFT involves a simple polymerization process that yields polymers with well-defined properties such as molar mass distribution, compositions, shapes and architectures. Significant advances have made RAFT polymerization an excellent process for the new generation of polymeric materials.[56,57] Indeed, RAFT polymerization technique has been used for the development of gene delivery vectors.[58] This technique has allowed an easy synthesis of suitable cationic polymers with pendent biocompatible moieties which are promising non-viral gene delivery vectors. A significant control

http://dx.doi.org/10.1039/D0PY01293A

in the design of cationic polymers *via* the RAFT process has allowed structure–activity relationship studies between these polymers and gene expression.[58] Several reviews have already been published on the mechanism of RAFT polymerization, monomers variety, bioconjugation strategies and on their biological applications.[59-61] Furthermore, a detailed study of biocompatibility and cytotoxicity for the use of these RAFT synthesized polymers for biological applications has shown that the toxicity of RAFT based polymers depends on the type of chain transfer agent (CTA) used for the synthesis, on the type of cell line used for the studies, and on the type of functional units present in the polymer.[58,62,63]

In our laboratory, we are interested in the use of positively charged ELPs for polyelectrolyte complexes formation to transport and deliver genetic material. Low immunogenicity, biocompatibility and minimal cytotoxicity are some of the desired properties of cationic polymers to become a better alternative than viral or lipid vectors.[64] Polylysine, polyethylenimine (PEI) and chitosan have been, up to now, the most commonly studied polycationic entities for DNA compaction.[65,66] PEI is considered as the standard for gene expression assays, both *in vitro* and *in vivo.*[67] PEI promotes high gene expression *in vitro* thanks to its efficient DNA complexation, high proton sponge effect, ,and facile DNA release, among others.[68,69] Nevertheless, the high cytotoxicity of synthetic cationic polymers and the low gene expression with polysaccharide-based complexes have opened new research opportunities to synthetize biocompatible cationic polymers for efficient nucleic acids delivery.[64,70] In a previous contribution, we have described the synthesis of positively charged ELPs through a two steps post-modification of a recombinant ELP, $(VPGXG)_{40}$ with X = V,M (3:1), to introduce chemoselectively either primary or secondary amine pendant groups at each methionine residue.[71] These ELPs were found to be able to interact with plasmid DNA and to form stable complexes for gene delivery. Furthermore, preliminary *in vitro* testing on HEK 293 cells viability showed that the modified ELPs complexed with DNA were non toxic to these cells. It was also found that ELPs containing periodically spaced cationic residues represent an attractive class of biopolymers for complex formation and nucleic acids delivery due to the possibility of modulating and quantifying the number of cationic charges. Hence, the introduction of other types of positively charged groups, such as small cationic peptides or cationic oligomers should be possible through this dual recombinant/synthetic modification approach. This will allow tuning ELP's complexation efficiency and pKa for the development of nanoparticles with various stability profiles.

In this contribution, hybrid cationic ELPs for nucleic acids transport and delivery were synthetized through the coupling of RAFT polymerization and biorthogonal chemistry of ELPs with the aim of introducing a higher number of positive charges to the ELP backbone, as well as modulating the charge density. For this, a series of cationic oligomers with variable lengths was prepared from a positively charged methacrylic monomer ([2-(methacryloyloxy) ethyl] trimethylammonium chloride, TMAEMA). These oligomers were synthesized by RAFT polymerization using a transfer agent containing an azido group. An ELP with the sequence $(VPGXG)_{40}$ with X=V,M (3:1) was produced recombinantly in *Escherichia coli* and purified from the cytoplasmic soluble fraction by the inverse transition cycling method.[34] Methionine residues of $(VPGXG)_{40}$ were then chemoselectively modified using an oxaziridine derivative to introduce alkyne groups and ultimately the cationic oligomers by copper-catalyzed azide-alkyne cycloaddition (CuAAC, Huisgen cycloaddition reaction). Three P(TMAEMA) oligomers with polymerization degrees of 6, 9, and 15 were grafted onto the ELP to access a small library of hybrid cationic ELPs. These were characterized by ^{1}H NMR, SEC and ζ-potential techniques to assess their purity and determine the degree of functionalization, molar mass and net charge. The study of the complexation process between these hybrid cationic ELPs and genetic material (plasmid DNA) was carried out in order to find the optimal conditions for obtaining stable nanoparticles having a controlled size and surface potential. Finally, preliminary biological tests were undergone to assess the reliability of such hybrid ELPs-oligomers cargo to internalize efficiently DNA into living cells.

B. Experimental

Materials

pUC19 DNA plasmid was purified from an *E. coli* culture using the Midiprep Macherey Nagel kit according to the manufacturer's instructions. The purified pUC19 plasmid was dissolved in deionized sterile water, and its purity and concentration were determined by UV spectrophotometry. NaOH in pellets with impurities ≤ 0.001 %, anhydrous NaCl, LB medium, glacial acetic acid, hexafluoroisopropanol (HFIP), N,N,N′,N′′,N′′-pentamethyldiethylenetriamine (PMDETA), potassium hydroxide, magnesium sulfate (≥ 99.99%), diethyl ether, 4-cyano-4-(phenylcarbonothioylthio)pentanoic acid (CPDB) RAFT agent, [2-(methacryloyloxy)ethyl]trimethylamonium chloride monomer (TMAEMA, 80 wt.% in H2O), 3-bromo-1-propanol, sodium azide, *N*-(3-dimethylaminopropyl)-N′ethylcarbodiimide hydrochloride, 4-dimethylaminopyridine and 4,4′-azobis(cyanovaleric acid) (ACVA) were purchased from Sigma-Aldrich (FR) and used as received (except the TMAEMA monomer that was passed through an inhibitor removal column prior to use). Fluorescein 5-isothiocyanate (FITC) (≥90%) was purchased from Sigma-Aldrich (FR). Oxaziridine-alkyne was home-made.[72] Bacto-tryptone and yeast extract were purchased from Biokar Diagnostics (FR). Ampicillin was obtained from Eurobio (FR). Glycerol and isopropyl β-D-thiogalactopyranoside (IPTG) were purchased from Euromedex (FR). Complete mini EDTA-free protease inhibitors were supplied by Roche Diagnostics (D). Deionized water (18 MΩ-cm) was obtained by passing in-house deionized water through a Millipore Milli-Q Biocel A10 purification unit. Cuprisorb was purchased from Seachem (USA). Acetonitrile (99.9%, ACN) was obtained from VWR international (FR). N,N′ Dimethylformamide anhydrous (99.8 %, DMF) and

http://dx.doi.org/10.1039/D0PY01293A

dichloromethane anhydrous (≥99.8%, DCM) were purchased from Sigma-Aldrich (FR). NaCl (99%) was purchased from Alfa Aesar (FR). Ammonium Acetate and Sodium ascorbate were purchased from Fisher Scientific (FR). Bioproduction, isolation and purification of the recombinant ELP with the primary sequence MW[VPGVGVPGMG(VPGVG)$_2$]$_{10}$ was accomplished following previously reported procedures.[34] Mammalian HEK293 cells (FreeStyle 293-F Cells, ref. R790-07), serum free medium (FreeStyle 293 expression medium, ref. 12338018), six well Nunc culture plates (Ref. 150239) and Hoechst 33342 (Ref. 62249) were purchased from ThermoFischer Scientific. Polyethylenimine (PEI 25 kDa, Ref. 23966 lot 661897) was purchased at Polysciences. Phosphate buffer saline (PBS) 0.01 M phosphate buffer, 0.0027 M potassium chloride and 0.137 M sodium chloride, pH 7.4 (Ref. P4417) were purchased at Sigma-Aldrich.

Production of ELP and modifications using oxaziridine-alkyne

ELP was produced following a previously reported method.[34] A solution of oxaziridine-alkyne (40 mg, 198 µM) in DMF (400 µL) was added to an ELP solution (50 mg, 2.9 µM) prepared in degassed water (50 mL) under N_2 atmosphere. After stirring for 30 mins, DCM (20 mL) was added and the mixture was extracted with DCM for two times to remove the benzaldehyde. The combined water layer was then dialyzed (15kD MW cut-off) against Milli Q water for 12h (changing water every 4 h). The final product was obtained by lyophilization.

Details of ELP(alkyne): ^{1}H NMR (400 MHz, D_2O, 25°C): (main peaks) δ 4.47–4.40 (m, 80 H, CHα Val and Pro, <u>V</u>PGXG), 4.18-4.17 (d, 30 H, CHα Val, <u>V</u>PG<u>V</u>G), 3.13-3.01 (m, 22 H, CH_2 Met signal l), 2.73 (s, 33 H, SCH_3 Met), 2.58 (t, 11 H, CH-Alkyne, signal β), 1.00-0.93 (br m, 420 H, CH_3 Val). Yield = 94 %.

Synthesis of cationic oligomers poly (TMAEMA) using the azido-RAFT agent

In a typical RAFT homopolymerization experiment, TMAEMA monomer (0.8 g, 10 eq, 3.85 mmol), ACVA initiator (22 mg, 0.2 eq, 0.077 mmol), and azido-RAFT agent (140 mg, 1 eq, 0.385 mmol) were pre-mixed in a vial along with 1 g of methanol and 0.2 g of H_2O (contained in the monomer) and then into a Schlenk flask. The solution mixture was degassed with five freeze-evacuate-thaw cycle and polymerized at 75°C. 77.7% monomer conversion was achieved in 2 hours as determined by ^{1}H NMR. The oligomer was then dialyzed against deionized water using a 500-1000 Dalton membrane (spectrum lab) for 24 hours with 5 changes of water.

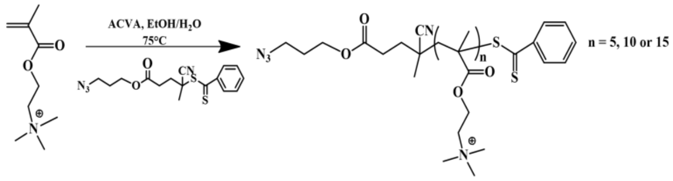

Scheme 1. Synthesis of cationic oligomers by RAFT polymerization of [2-(methacryloyloxy)ethyl]trimethylamonium chloride monomer (TMAEMA) in MeOH using the azido RAFT agent and initiated by ACVA at 75 °C.

After freeze drying, the red powder obtained was characterized by aqueous SEC, ^{1}H NMR and IR to measure respectively the degree of polymerization (*DP_n*, **Fig. 1**), the polydispersity index (*Đ,* **Fig. 2** and **Table 1**) and the presence of the N_3 stretching band of the azide group (2100 cm^{-1}, **Fig. S2**).

Details of cationic oligomers poly (TMAEMA): ^{1}H NMR (400 MHz, D_2O, 25°C): (main peaks) δ 7.90–7.25 (m, 5 H, C_6H_5 phenyls groups RAFT agent), 4.5-4.25 (m, 12.3 H, O-<u>CH$_2$</u>-CH$_2$-N(CH$_3$)$_3$ monomer), 3.95-3.55 (m, 12.9 H, O-CH$_2$-<u>CH$_2$</u>-N(CH$_3$)$_3$ monomer). DP_n = 6, Yield = 70 %.

ELP-cationic oligomers coupling

The alkyne-bearing ELP derivative obtained from oxaziridine functionalization was dissolved in a mixture of EtOH 75% (5 mg/mL) and one of the three possible cationic oligomers (DP= 15, 9 and 6); 1.5 equiv. per alkyne were added. The solution was degassed by bubbling N_2 for 2 hrs and then stirred under N_2. Separately, a solution of Cu(I) was prepared by addition of sodium ascorbate (20 equiv. per alkyne) to a degassed solution of Cu(II)SO$_4$ (2 equiv. per alkyne) and pentamethyldiethylenetriamine (2 equiv. per alkyne). The Cu(I) solution was transferred to the reaction mixture with a syringe. The reaction was stirred under N_2 at room temperature for 72 hrs, Cuprisorb (100 mg), a powerful absorbent of copper, was added to the reaction mixture and stirred for 48 hrs. Cuprisorb beads were separated by centrifugation and the supernatant was transferred to a 10 kDa MWCO dialysis bag and dialyzed against EtOH 75% during 4 days with 4 solvent changes, followed by 24 h dialysis against DI water with 3 changes. The purified reaction mixture was then lyophilized to provide the hybrid cationic ELP as a brown solid.

Details of cationic hybrid ELPs: ^{1}H NMR (400 MHz, D_2O, 25°C): (main peaks): δ 8.0-7.8 (br s, 11 H, triazole-H), 4.18-4.17 (d, 30 H, CHα Val, <u>V</u>PG<u>V</u>G), 2.73 (s, 33 H, SCH_3 Met), 3.40-3.20 (m, N(CH$_3$)$_3$ oligomer), 1.03-0.82 (m, 420 H, CH_3 Val). Yield = 80 %.

DNA and ELPs solutions preparation

The purified pUC19 plasmid was diluted up to 1 mg/mL in deionized sterile water and dilutions up to 0.005 mg/mL were prepared with a Tris 10 mM buffer (pH=7.4). Cationic hybrid ELPs solutions were prepared at a concentration of 0.2 mg/mL by dissolving a known amount of ELP in water. All vials were closed and sealed with Parafilm® to prevent water evaporation. All solutions were stored at a temperature of 4 ºC.

^{1}H NMR analyses

^{1}H NMR analyses were performed in a Bruker AVANCE III HD 400 apparatus equipped with a 5 mm Bruker multinuclear z-gradient direct probe operating at 400.2 MHz for ^{1}H. An amount of 7 mg of ELP was dissolved in 0.5 mL of deuterated solvent (D_2O) and 128 scans were recorded. ^{1}H NMR spectra were acquired in D_2O and $CDCl_3$ at 298 K. The solvent signal was used as the reference signal (δ=4.79 ppm). Bruker Topspin Software was used to perform data processing. Chemical shifts of amino acids are well-known in the literature and were used to fully assign the obtained spectra.[74,75]

Size Exclusion Chromatography (SEC) analyses

SEC analyses of ELP, ELP derivatives and cationic oligomers were performed on a liquid chromatographic system from ThermoScientific equipped with two G4000PWXL and G3000PWXL gel columns (300 x 7.8 mm) (exclusion limits from 200 Da to 300 000 Da) and UV detector at a flow-rate of 0.6 mL/min. Columns temperature was maintained at 25 °C. The system includes a multi-angles light scattering detector MALS and differential refractive index detector dRI from Wyatt technology. Aqueous solvent composed by Acetic Acid (AcOH) 0.3 M, Ammonium Acetate 0.2 M and ACN (6.5/3.5, v/v) was used as the eluent. Ethylene glycol was used as flow marker. *dn/dc* measurements were performed on the differential refractive index detector dRI from Wyatt technology by injecting 500 µL of each sample dissolved in the aqueous buffer at 8, 10 and 15 mg/mL.

ζ-potential measurements

ζ-potential measurements were performed on a Malvern Zetasizer NanoZS at a temperature of 37 ºC. Firstly, ζ-potential measurements were performed in parallel to pH measurements to determine ELP derivatives isoelectric point in presence of an excess of HCl by progressive NaOH addition. DNA/Cationic hybrid ELPs complex formation was monitored by ζ-potential measurements upon the progressive addition of cationic hybrid ELP (0.2 mg/mL) into the DNA solution (0.005 mg/mL) at controlled pH (7.4), under continuous agitation. Slow dropwise mixing of cationic hybrid ELPs to a negatively charged DNA solution was selected as complex formation method.[71,76-78] The stabilization of pDNA/Cationic hybrid ELPs complexes was reached after 5 min. of each cationic ELP addition. Then, 1 mL of the mixture was transferred into the Zetasizer NanoZS cell for the measurement. The sample was transferred back into the initial solution after each measurement before the next addition of cationic hybrid ELP. In this way, a nearly constant volume of ELP/DNA complex solution was maintained. Net charge of pDNA/Cationic hybrid ELPs was also determined through ζ-potential measurements. The electrophoretic mobility of the particles was measured by the instrument and then converted to the ζ-potential using the classical Smoluchowski expression.[79]

Dynamic light scattering (DLS) measurements

Dynamic light scattering (DLS) measurements were performed on a Malvern ZetaSizer Nano ZS instrument equipped with a standard HeNe laser emitting at 632.8 nm (Malvern, U.K.) at a 90° angle with a constant position in the cuvette (constant scattering volume). An amount of 100 mL of DNA/Cationic hybrid ELPs complex was introduced in a high precision quartz cell with a light path of 3x3 mm^2. The stabilization of the complexes was reached after 5 min. The correlation functions were averaged from three measurements of 10 runs (30 s each one) at a temperature of 37 °C after a 2 min-temperature equilibration time. The Stokes−Einstein equation proposed for spherical particles was used to determine as a first approach the corresponding hydrodynamic radius of the complexes.[80]

Agarose gel electrophoresis

DNA/Cationic hybrid ELPs binding assays were assessed through gel retardation assays by mixing 100 ng of pUC19 plasmid with increasing amounts of ELPs derivatives (0.2 mg/mL) in 20 µL of a mixture of buffer (5% glycerol, 1mM EDTA, 10mM Tris–HCl pH of 87.4, 1mM dithiotreitol and 20 mM KCl) and water (at 1/9 v/v ratio). DNA/Cationic hybrid ELPs complexes were stabilized under stirring during 30 min at room temperature. An amount of 3 µL of loading buffer (0.1 mM EDTA, 0.05% bromophenol blue, 50% glycerol) was added to the mixture and an aliquot of 10 µL was applied to a 1.2 % agarose gel electrophoresis prepared in 1x TAE buffer (40 mM Tris, 20 mM Acetic acid, 1 mM EDTA). SYBR® Safe (Life Technologies, Carlsbad, CA, USA) was used to reveal the DNA bands.

Atomic force microscopy (AFM) measurements

AFM measurements were carried on at room temperature in a dry state using a Multimode 8™ microscope (Veeco Instruments Inc.). Tapping Mode ™ using rectangular silicon cantilever (AC 160-TS, Atomic Force, Germany) was selected to obtain phase and topographic images of individual particles. A spring constant of 26 N/m was used. A resonance frequency lying in the 270-320 kHz range and a radius of curvature of less than 10 nm were selected for the measurements. Samples were prepared by solvent casting at ambient temperature from a DNA/Cationic hybrid ELPs complex mother suspension having a concentration of 0.03 mg/mL for pDNA. A drop (4 µL) of suspension was deposited onto freshly cleaved mica and allowed to dry under nitrogen flow during several minutes. Diameter and height measurements were taken using the section Particle Analysis tool provided with the AFM software (Nanoscope Analysis V1.20 from Bruker).

Transmission Electron Microscopy (TEM)

TEM images were obtained on a Hitachi H7650 microscope equipped with an Orius SC1000 11 MP camera performing at 80 kV. Samples were prepared by direct deposition of a 10 mL droplet of hybrid-ELP/pDNA complex sample on carbon grids (300 mesh, Cu-300LD from Pacific Grid Tech). After 10 min, excess of liquid was blotted using a filter paper. Samples with different charge ratios (R= N^+/P^-) were imaged. The particle size distribution was measured using ImageJ software one-by-one.

Fourier-transform Infrared Spectroscopy (FTIR)

FTIR measurements were performed in a FTIR Bruker Vertex 70 spectrometer at room temperature with an ATR Diamond point in Transmission mode. A drop of each sample of $P(TMAEMA)_{DP}$ oligomers (DP= 6,7,9,15) was used to perform each measurement. OPUS Software was used for data analysis.

Laser Scanning Confocal Microscopy (LSCM)

http://dx.doi.org/10.1039/D0PY01293A

Laser Scanning Confocal Microscopy Images were acquired on an inverted Leica TCS SP5 microscope equipped with an HCX PL APO 63x, NA 1.4 oil immersion objective in fluorescence mode. Samples (≈50 µL) were injected in µ-slide (chambered coverslip) with uncoated 8 wells from Ibidi GmbH. The laser outputs are controlled via the Acousto-Optical Tunable Filter (AOTF) and the three collection windows using the Acousto-Optical Beam Splitter (AOBS) and photomultiplicators (PMT) as follows: Hoechst 33342 was excited with a laser diode at 405 nm (12.5%) and measured with emission setting at 410-510 nm, FITC was excited with an Argon laser at 488 nm (20%) while the emission was collected in the 500-570 nm range, and cells were excited with a Helium-Neon laser at 633 nm (10%) in transmission mode. Images were collected using the microscope in sequential mode to avoid the overlapped emission with a line average of 4 and a format of 512*512 pixels.
Photomutliplicators gain and offset configurations were set up on control cells so as to correct images from green auto-fluorescence signal. A Z-stack of 60 frames covering a depth of 40 µm was recorded at 400 Hz for assessment of label distribution across the section. Processing of fluorescence confocal acquisitions and 3D reconstruction were performed using the ImageJ software.

Biological experiments

FITC-pDNA labeling

DNA plasmid tagged with fluorescein was prepared according to the method established by *Ishii et al*.[81] The schematic reaction for this synthesis is shown in **Scheme S2**. FITC-benzylamine was synthetized by reacting fluorescein isothiocyanate (FITC, 0.257 mmol) and 2-(4-aminophenyl)-ethylamine (0.257 mmol) in 1.5 mL of DMF. FITC was used without further purification. This reaction was carried out overnight at 25 °C under stirring. The proceeding of the reaction was monitored by silica gel chromatography. The elution solvent was a mixture of cyclohexane and ethyl acetate (2:8, v/v). The spots of the following compounds: fluorescein isothiocyanate (R_f=0.74) and 2-(4-aminophenyl)-ethylamine (R_f=0.1), completely disappeared and the new spot of FITC-benzylamine (R_f=0.26) appeared. The structure of compound FITC-benzylamine was analyzed by direct infusion mass spectroscopy (DIMS) inside a LTQ XL from Thermoscientific, where $[M+H^+]$=526 (**Fig. S3**), in good agreement with the literature. FITC-diazonium salt was then prepared by reacting FITC-benzylamine (25.7 µmol in 150 µL of DMF) with sodium nitrite (110 µmol) in 2 mL of 0.5 M HCl for 5 min at 0 °C under stirring. The reaction was stopped with the addition of 1 mL of 1 M NaOH. Then, the solution of FITC-diazonium salt (25 µmol) was mixed with a solution of DNA plasmid (0.315 mg) in 15 mL of 0.1 M borate buffer (pH 9.0). The reaction was carried out for 15 min at 25 °C under stirring. The FITC-labeled plasmid was then purified with the NucleoSpin Gel and PCR Clean-up kit (Macherey nagel) according to the manufacturer's instructions, and analyzed through agarose gel electrophoresis.

Mammalian cell transfection

HEK293 suspension cells were cultivated in 6 well plates, at 37 °C, 100 rpm, 8% CO2, in serum free medium with a 2 mL culture volume. Cells were transfected (i) with FITC-pDNA/ELP-$P(TMAEMA)_{15}$ complexes prepared at charge ratio $N^+/P^=$ of 5, 10 and 23, (ii) with FITC-pDNA/PEI complexes prepared at a N^+/P^- ratio of 23 as a positive control, as transfection conditions are described as efficient,[82] or (iii) without any complexes as negative control. In-house ADV-1 control plasmid (4.7 kb) was used as pDNA source. Solutions of ELP-$P(TMAEMA)_{15}$ derivatives were prepared at 2 mg/mL in DI water (final pH around 6.0). Polyethylenimine (PEI) was dissolved in distilled water at 1 mg/mL and adjusted to pH 7. Briefly, cells were passaged every 2-3 day in serum free medium. At day before complexes addition, cells were passaged at 1 million cell/mL. At transfection day, cell viability was over 90%. pDNA and polymers were prior conditioned in PBS and complexes were prepared at ratios mentioned above and added to cells at 1 µg pDNA per million cells with an addition of 10 % v/v. Cell suspension was sampled readily after transfection at 30 minutes, 4, 24 and 48 hours later. A volume of 100 µL of cells was harvested and centrifuged (5 min, 300 g). Cell pellets were resuspended and incubated 5 min at 37°C with 100 µL of Hoechst 33342 reagent (2 µg/mL) for nucleus staining. Reagent was removed by centrifugation (5 min, 300 g) and cells were re-suspended in 400 µL of PBS then analyzed by Laser Scanning Confocal Microscopy (LSCM) and cytometry.

Cytometry analysis

Cell suspensions were injected on a cytometer (Accury C6, BD Biosciences) for cell distribution, viability and fluorescence analysis. FITC was excited with a 488 nm laser and fluorescence was recorded on FL1 channel (533/30 nm). FITC fluorescence of cells was analyzed as follow. A first screen of FSC-A according to time were plotted in order to detect any dysfunction or heterogeneity during injection. Then, the events FSC-H were plotted according to FSC-A in order to detect and to eliminate doublets or larger cell aggregates if required. The events were then gated as depicted in **Fig. S4**. On the negative control assay (untransfected cells), the population of cells was selected in order to discard small debris and artifacts. Thereafter two gates were defined to sort "Alive" or "Dead" cells. Finally, the "Alive" gated cells were analyzed according to their fluorescence intensity. The negative control sample was the reference to set the limit for non-fluorescent cells (left hand) or fluorescent cells (right hand). Gates and limits defined on negative control sample were applied for all samples.

C. Results and discussion

Synthesis of RAFT oligomers bearing an azide group at the chain end

To be able to tune the number of positive charges of the hybrid cationic ELPs, a grafting onto approach was considered by clicking the RAFT-synthesized PTMAEMA oligomers bearing an azide group onto the alkyne modified ELP. A series of four cationic oligomers were obtained by RAFT using a chain transfer agent (CTA) modified by esterification to contain an azide function on its R group (see **Scheme S1** and **Fig. S1**). The aim was to tailor the number of charges provided by the TMAEMA monomer while keeping the degree of polymerization of the oligomers low enough to have controlled positives charges (between 44 and 100) on the final ELP-oligomer carriers. As published in a previous contribution, positively charged ELPs bearing 22 charges per chain were already found to be able to interact with plasmid DNA and form complexes with an average ζ-potential of +15 mV for gene delivery. Other polycations such as chitosan78 or as the highly positively charged poly(ethylenimine) (PEI), can destabilize cell membrane at high charge ratios.71,78 Even though, highly charged polycation PEI is one of the most potent non-viral polymeric gene vectors and is used as positive control in many transfection assays.

This was achieved by targeting low DP for the oligomers, and by avoiding the polymerization to reach full conversion. **Fig. S2** represents the evolution in Size Exclusion Chromatography (SEC) of the trace of the monomer to a trace of an oligomer. Here it is possible to observe a notable shift of the TMAEMA peak to higher molecular weights when compared with the P(TMAEMA)15 oligomer, showing that even at low DPs this increase is evident with SEC technique. However, it can be noticed that at these low target DPs (see **Table 1**), the RAFT CTA is only around 50 % efficient, which means that for a DPt = 5, a DP at 100 % conversion of 10 should be obtained. Such inefficiency of the RAFT CTA has already been calculated and reported.[83] Moreover, the discrepancy is here enhanced for targeting oligomers where the CTA efficiency varies between 39 up to 61 %, as seen in the **Table 1**.

The reaction time was adapted to obtain relatively low monomer conversion for the two targeted DPs of 10 and 5. It is expected that unreacted RAFT CTA will be present at the end of the polymerization. However, they will be removed by purification (*i.e.* dialysis). The conversions were calculated by ^{1}H NMR analyses by integrating the amount of residual monomer compared to the polymer formed. The dithiobenzoate RAFT CTA used was chosen since it controls correctly the polymerization of methacrylates, it is commercially available and the phenyl group can easily be quantified when analyzing the purified oligomers and then allows to accurately calculate the DP by ^{1}H NMR.

Table 1. Molecular characteristics of the P(TMAEMA)$_x$ oligomers with x = 6, 7, 9 and 15.

Target DP	Reaction time (min)	Conversion (%)	DP calculated from ^{1}H NMR	M_n from ^{1}H NMR (g/mol)	M_n from GPC (PEG calibration) (g/mol)	M_n from MALS dn/dc = 0.1039 (g/mol)	Đ from SEC	CTA efficiency (%)
10	120	78	15	3 478	1 330	7 570	1.074	52
10	50	55	9	2 232	1 240	5 890	1.017	61
5	90	71	7	1 816	1 200	5 250	1.024	51
5	45	47	6	1 609	1 100	4 700	1.013	39

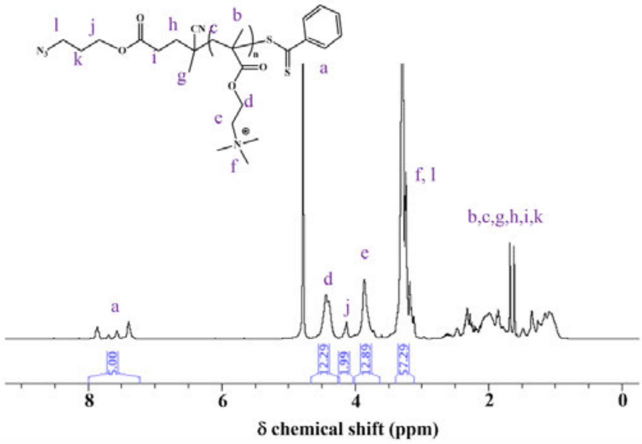

Fig. 1. ^{1}H NMR spectrum of P(TMAEMA)$_6$ in D_2O (25 °C, 400.2 MHz).

As an example, **Fig. 1** presents the ^{1}H NMR spectrum of a cationic PTMAEMA oligomer having a DP of 6. Using the resonance peaks at 7.25- 8 ppm corresponding to the phenyl protons from the CTA (5 ^{1}H) as reference, resonance peaks corresponding to the oligomeric segment were integrated, namely the two protons O-C$\underline{H}_2$-CH$_2$-N(CH$_3$)$_3$ (12.29 ^{1}H, 4.25-4.60 ppm), the two protons O-CH$_2$-C$\underline{H}_2$-N(CH$_3$)$_3$ (12.89 ^{1}H, 3.70-4.00 ppm) and the nine protons O-CH$_2$-CH$_2$-N(C$\underline{H}_3$)$_3$ (57.29 ^{1}H, 3.45-3.10 ppm) from the TMAEMA monomer. This gives an average DP of 6 for this polymer by end group analysis.

The different cationic PTMAEMA oligomers were analyzed by size exclusion chromatography (SEC) using two detectors (RI and SEC-MALS) to confirm molar mass shifts between the oligomers with the lowest and highest DPs. (**Fig. 2**) SEC results were examined through the comparison of the RI signal with PEG standards (**Table 1)**. There is a discrepancy between the value of the M_n obtained by SEC and the ones calculated by ^{1}H NMR: this is due to the PEG calibration that is providing lower M_n than the one expected. However, as mentioned earlier, the SEC M_n were observed in the right order depending on the DP (and by extension the M_n) obtained by ^{1}H NMR. The relation between the DP and the M_n by ^{1}H NMR is given by the relation M_n = $M_{monomer}$ * DP + M_{CTA} = 207.7*DP + 362.47. The synthetized oligomers present a narrow polydispersity index and molar masses increased in accordance with the calculated DP by ^{1}H NMR. Further attempt to determine cationic oligomers molar masses from SEC measurements was performed by using the multi-angle light scattering detector. dn/dc values were used to assess to this information. The Mn values determined through this method were also observed in

http://dx.doi.org/10.1039/D0PY01293A

the right order depending on the DP (and by extension the Mn) obtained by 1H NMR. However, they show also a discrepancy if compared to the calculated values by 1H NMR, this could be presumable related to the retention of an important % of product in the columns and possible electrostatic associations, increasing the Mn value 2 or 3 times.

Furthermore, the infra-red spectra of the cationic PTMAEMA oligomers shown in **Fig. S3** exhibited a clear band at 2100 cm^{-1}, corresponding to the azide group present on the R group and resulting from the CTA in the oligomers. To summarize, four cationic PTMAEMA oligomers, clickable at their chain end through the azide groups and presenting a low polydispersity index were synthetized through RAFT polymerization. The different DP values ranging from 6 to 15 were determined through ^{1}H NMR (**Fig. 1**, **Fig. S6**, **S7** and **S8**).

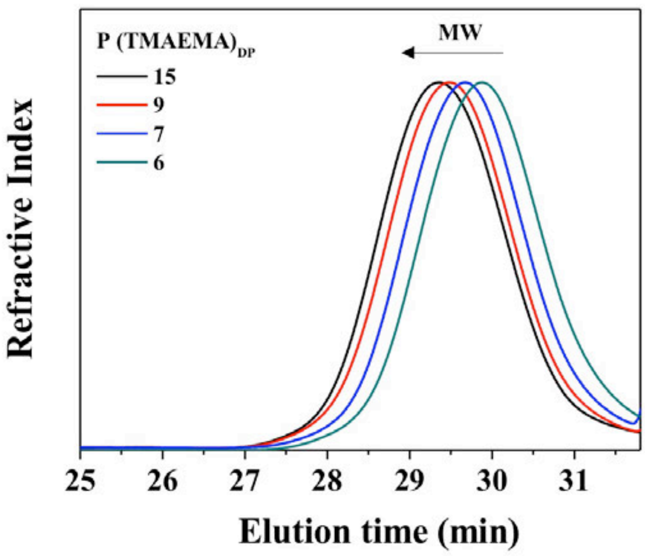

Fig. 2. Size exclusion chromatograms in AcOH/Ammonium Acetate/ACN of $P(TMAEMA)_x$ oligomers with x = 6 (green), 7 (blue), 9 (red) and 15 (black).

It is worth mentioning that RAFT technique has been used to synthetize polymers with molar masses up to 100 000 g/mol, being achievable while keeping control over dispersity and end-group functionality.[84] However, DP lower than 15 are not common to find in the literature due to the lack of control of the RAFT polymerisation for poly(methacrylate) at the beginning of the reaction. Such results were found by Derry *et al.*[85] for their polymerization of low DP of poly(stearyl methacrylate) (PSMA). For a targeted $PSMA_5$, a $PSMA_{13}$ was obtained at 76% of monomer conversion, which in this case is also a very low efficiency for this dithiobenzoate RAFT agent.

Moreover, as an example for common low DP values, Das *et al.* synthesized glycopolymers with a targeted degree of polymerization (DP) of 35 (molar mass = 9,951 g/mol) and 350 (molar mass = 97,206 g/mol) by aqueous RAFT (aRAFT) polymerization.[86] Concerning the intracellular delivery of nucleic acids, since recent results showed that amphiphilic polymers incorporating quaternary amine groups cause pH-independent cell lysis[87], comb-like polymers poly(HMA-*co*-TMAEMA) with 53 to 69 number of TMAEMA units per graft/ Comb-like Polymer (684 to 1330, respectively) were synthetized by Lin *et al.* [88] Therefore, an exquisite control of dispersity combined with low DP, as obtained in this work, will give the possibility to introduce a controlled number of positive charges in the ELP backbone.

Synthesis of 'clickable' ELPs modified with alkyne groups

The native recombinant ELP[M_1V_3-40] corresponding to the sequence $(VPGXG)_{40}$, where X=V/M (3:1), here simply referred to as ELP (**Fig. 3a**)[34,71], was chemoselectively modified onto methionine residues in order to graft in a second step the cationic PTMAEMA oligomers. **Fig. 3b** presents a schematic representation of the attachment of cationic PTMAEMA oligomers onto a chemoselectively post-modified ELP presenting periodically spaced alkyne groups. Recently, our research group reported the chemoselective modification of methionine-containing ELPs using oxaziridine derivatives.[72] This synthetic approach was used here to introduce alkyne groups on the side chain of each methionine residue of the ELP (11 total in the sequence) (**Fig. 3c**). The degree of functionalization was determined by ^{1}H NMR spectroscopy (**Fig. S9-10**) ^{1}H NMR spectra were calibrated using the resonances centered at 4.45 ppm, which correspond to the αC*H* protons of the first valine in each (VPGXG) repeat and to the αC*H* protons of proline, integrating as 80 protons total.

Integration of the resonance peak at ca. 2.58 ppm, corresponding to the acetylene protons, was used to determine the degree of functionalization (full functionalization corresponds to 11 protons). A complete functionalization of ELP(Alkyne) was obtained at this step (**Fig. S10**).

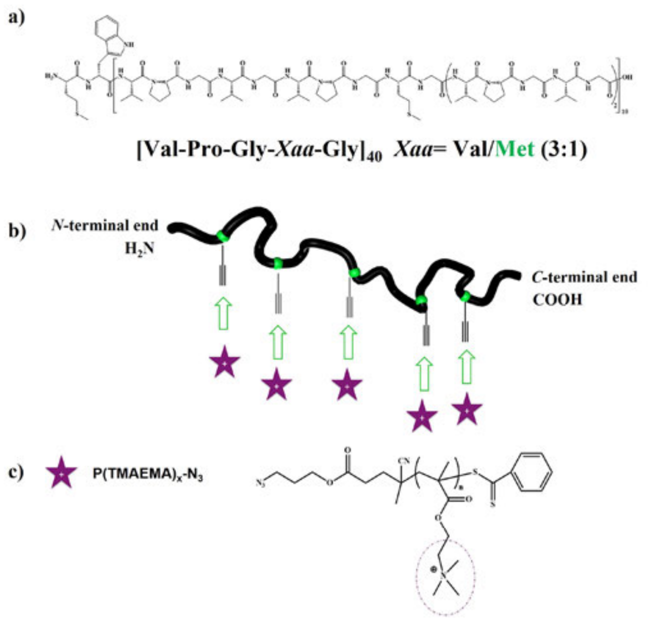

Fig. 3. a) Chemical structure of the native ELP, b) schematic representation of the grafting of oligomers onto ELP backbone

http://dx.doi.org/10.1039/D0PY01293A

by Huisgen cycloaddition to obtain the nucleic acids nanocarriers.

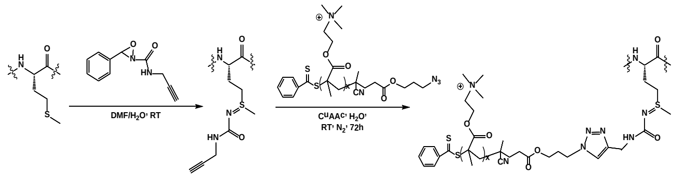

Scheme 2. Simplified reaction scheme of the synthesis of cationic hybrid ELPs, ELP-*g*-P(TMAEMA)$_x$, where x=6, 9 or 15.

Coupling of RAFT oligomers and modified ELPs: synthesis of cationic hybrid DNA carriers

Huisgen cycloaddition was chosen as the click reaction between the RAFT cationic oligomers bearing an azide group and the alkyne modified ELP to obtain the hybrid ELP-*g*-P(TMAEMA)$_x$ derivatives. The CuAAC reaction was achieved using similar conditions to those described by Bravo-Anaya *et al.* for the modification of alkyne-functionalized ELPs with amino groups (*i.e.,* EtOH 75%, Cu(II)SO_4, sodium ascorbate, PMDETA).[71] A reaction time of 72 h and excess reagents of 1.5 equiv. azido-oligomers per Met residue was necessary to maximize the coupling onto ELP(-CCH). **Fig. 4** shows, as an example, a detailed ^{1}H NMR spectrum of ELP-P(TMAEMA)$_6$, where it is possible to visualize the protons from the cationic oligomers and the protons from the modified ELPs. ^{1}H NMR spectra were calibrated using the resonance peak centered at 0.82-1.03 ppm, which corresponds to the methyl protons of Val residues, integrating as 420 protons total (**Fig. S9, S10** and **S11**). The appearance of the resonance at 7.8-8.0 ppm and at 3.20-3.40 ppm is attributed to the proton of the triazole ring and to the protons of the cationic oligomers, $N(C\underline{H}_3)_3$, respectively (**Fig. S12** and **S13**). Integration of the resonance at ca. 7.9-8.0 ppm, corresponding to the triazole ring of ELP-*g*-P(TMAEMA)$_x$ was used to determine the degree of functionalization (full functionalization corresponds to 11 protons).

Three cationic hybrid ELPs were therefore synthesized, namely ELP-*g*-P(TMAEMA)$_6$, ELP-*g*-P(TMAEMA)$_9$ and ELP-*g*-P(TMAEMA)$_{15}$, using the cationic oligomers with the DP of 6, 9 and 15, respectively. They were analyzed using different techniques to confirm their molar masses, determine their isoeletric points (IP), total number of charges and thermal responsiveness. Through ^{1}H NMR measurements, functionalization degrees after click chemistry were found to be 70 % for ELP-*g*-P(TMAEMA)$_6$, 66 % for ELP-*g*-P(TMAEMA)$_9$ and 57 % for ELP-*g*-P(TMAEMA)$_{15}$. Incomplete functionalization was attributed to steric hindrance and charge repulsion between PTMAEMA oligomers, the longer the oligomer, the lower the functionalization. Similar phenomena were observed during the grafting of functional end groups to cellulose nanowhiskers (CNWs), an acid-hydrolyzed form of native cellulose. Grafting polymer chains or functional end groups of macromolecules to hydroxyl groups on the CNW surface has been done using the "graft onto" strategy, which includes isocyanation, esterification, silylation and click chemistry. However, it was reported that it was not possible to expect high grafting densities due to steric hindrance and blocking of reactive sites by the already grafted polymer chains.[89]

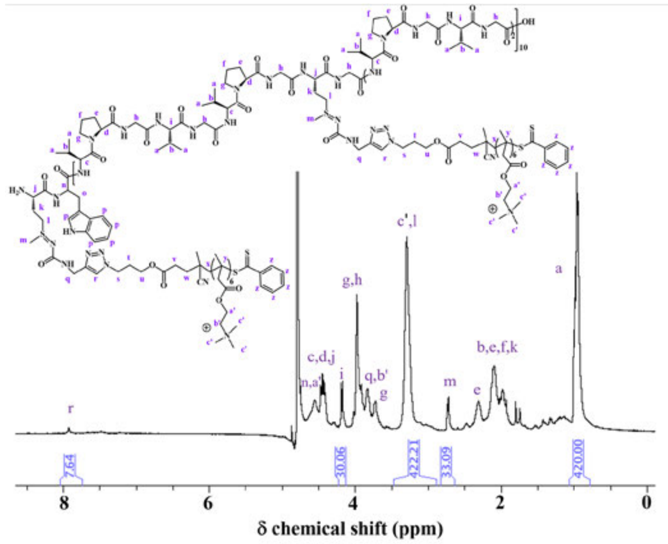

Fig. 4. Detailed ^{1}H NMR spectrum of the cationic hybrid ELP-*g*-P(TMAEMA)$_6$ in D_2O (25 °C, 400.2 MHz).

The molar mass changes of each ELP derivative after the different chemical modifications were followed by SEC analyses in aqueous solvent (acetic acid 0.3 M, ammonium acetate 0.2 M / ACN; 6.5/3.5, v/v). SEC traces showed expected shifts for each ELP derivatives and the obtained cationic hybrid ELP (**Fig. 5, Fig. S14-15**). SEC analyses showed the narrow distribution of the P(TMAEMA) oligomers and allowed to assess the efficiency of the click reaction between these two by an increase of molar mass between the alkyne-modified ELP and the ELP-*g*-P(TMAEMA) derivatives. The slight excess of P(TMAEMA) was removed by dialysis to obtain the final purified ELP-*g*-P(TMAEMA).

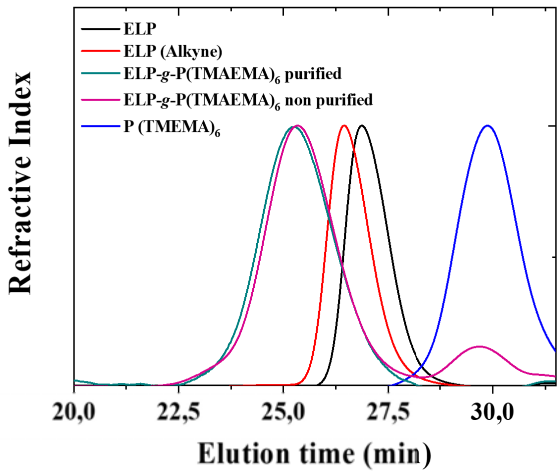

Fig. 5. Size exclusion chromatography traces in AcOH/Ammonium Acetate/ACN of ELP (black), ELP(Alkyne) (red), ELP-*g*-P(TMAEMA)$_6$ purified (green), ELP-*g*-P(TMAEMA)$_6$ non purified (pink) and P(TMAEMA)$_6$ (blue).

Table 2 summarizes the characteristics of ELP-*g*-P(TMAEMA)$_6$, ELP-*g*-P(TMAEMA)$_9$ and ELP-*g*-P(TMAEMA)$_{15}$. ζ-Potential measurements and potentiometric titrations were also carried in order to have information about cationic hybrid ELPs global charge and to evaluate their isoelectric point (IP).[90] As determined in a previous work, the experimentally determined IP for the native ELP is equal to 5.65, which is close to their theoretical IP, *i.e.* 5.27.[71,91] Alkyne-modified ELP presented an IP of 7.9. The IP of the cationic hybrid ELPs were found to be around 10.4, 11.7 and 11.8, for ELP-*g*-P(TMAEMA)$_6$, ELP-*g*-P(TMAEMA)$_9$ and ELP-*g*-P(TMAEMA)$_{15}$, respectively. These values are close to the ones reported for amine-containing ELP derivatives obtained by chemoselective thioalkylation.[71]

Table 2. *Characteristics of ELP derivatives. Molar mass determined by ^{1}H NMR and SEC measurements (using dn/dc), isoelectric point (IP) determined by potentiometric titrations and ζ-potential measurements.*

ELP Derivative	^{1}H NMR	Number of positive charges afforded by TMAEMA units[b]	SEC			IP
	Molar mass (g/mol)[a]		dn/dc[c]	MW (g/mol)[d]	*Đ* *from SEC*	
ELP	-	0	0.139	17,370	1.002	5.65
ELP(Alkyne)	18,091	0	0.136	18,040	1.002	10.36
ELP-g-P(TMAEMA)$_6$	30,383	46	0.120	31,190	1.078	10.39
ELP-g-P(TMAEMA)$_9$	34,340	66	0.120	34,020	1.025	11.77
ELP-g-P(TMAEMA)$_{15}$	40,002	95	0.120	36,120	1.044	11.79

[a] *Molar masses of ELP derivatives were estimated from ^{1}H NMR measurements taking the theoretical molar mass of the initial ELP (17,035 g/mol).[24] The % of functionalization was multiplied by 11 available methionine residues and by the molar mass of the respective cationic oligomer grafted for each coupling (P(TMAEMA)$_6$, P(TMAEMA)$_9$ and P(TMAEMA)$_{15}$), then added to the initial ELP molar mass.*

[b] *Number of positive charges afforded by TMAEMA units were calculated from H NMR results.*

[c] *dn/dc were determined by SEC measurements.*

[d] *Molar masses of ELPs derivatives were determined from SEC measurements by using a multi-angle light scattering detector. The intensity of the resulting scattered light from relaxation of the molecule (collected by the detector) was measured as the Raleigh ratio R_Θ, which is directly proportional to the molar mass of the solute molecule scattering the light. dn/dc values were used for this purpose.*

As shown in **Table 2**, these cationic hybrid ELPs have a charge density (number of positive charges) tunable through chemoselective post-modifications using the different positively charged oligomers with DP between 6 and 15. The ζ-potential of the cationic hybrid ELPs at pH 6.0 were 18±1, 21±1.0 and 24±0.5 for ELP-*g*-P(TMAEMA)$_6$, ELP-*g*-P(TMAEMA)$_9$ and ELP-*g*-P(TMAEMA)$_{15}$, respectively. Other polycations such as polyethylenimine (PEI),[92] poly-L-lysine (PLL)[93] and chitosan[66,78,90,94] have higher charge densities and tend to destabilize cell membrane at high N^+/P^- charge ratios. It is well known that this charge ratio strongly influences the nucleic acid nanocarrier's ζ-potential.[95] Highly positive net charge favors the colloidal stability of non-sterically stabilized complexes and enhances the interactions with the negatively charged cell membrane, leading to high cellular uptake and transfection efficiency *in vitro.* Nevertheless, despite the higher stability given by the high N^+/P^- ratio, excess of polycation can also lead to higher cytotoxicity, which in the case of siRNA led to a decrease in the amount of nucleic acid released.[96] Low N^+/P^- ratio complexes using cationic hybrid ELPs should then present a minimal impact on cell viability and can be an interesting alternative for nucleic acids delivery.

Finally, the effects of each chemoselective modification, *i.e.* alkyne introduction using oxaziridine derivatives and cycloaddition to graft positively charged PTMAEMA oligomers to the ELPs backbone, on the thermo-responsive behavior of the resulting ELPs were evaluated by dynamic light scattering (DLS) measurements. As expected, the presence of PTMAEMA oligomers in ELP-*g*-P(TMAEMA)$_6$, ELP-*g*-P(TMAEMA)$_9$ and ELP-*g*-P(TMAEMA)$_{15}$ resulted in the complete loss of thermal responsiveness (no detectable T_t) as a result of a greater hydrophilic character brought by quaternary amino groups.

Complexation of ELP-P(TMAEMA)$_X$ with nucleic acids

The mixture of oppositely charged polymers leads to electrostatic interactions between both types of polyelectrolytes followed by the formation of complexes with counterions release.[71,77,78,90,97] Hence, when positively charged ELP-*g*-P(TMAEMA)$_X$ was added under stirring into a dilute pDNA solution, an electrostatic complex was formed, as evidenced from ζ-potential measurements (**Fig. S16**), gel retardation, DLS, TEM and AFM measurements. **Fig. S16** presents the ζ-potential as a function of the total N^+ amount added and to a pDNA solution, expressed as N^+/P^-. pDNA molecules in solution give an initial ζ-potential of around -45±3 mV, which reaches the ζ-potential=0 mV, corresponding to the isoelectric point (IP) of the complexed particles, during the progressive addition of ELP-*g*-P(TMAEMA)$_X$ (with x=6, 9 or 15). For ζ-potential values higher than 0 mV, it is possible to observe a plateau corresponding to an excess of ELP-*g*-P(TMAEMA)$_X$ in the pDNA/ELP-*g*-P(TMAEMA)$_X$ complex suspension.

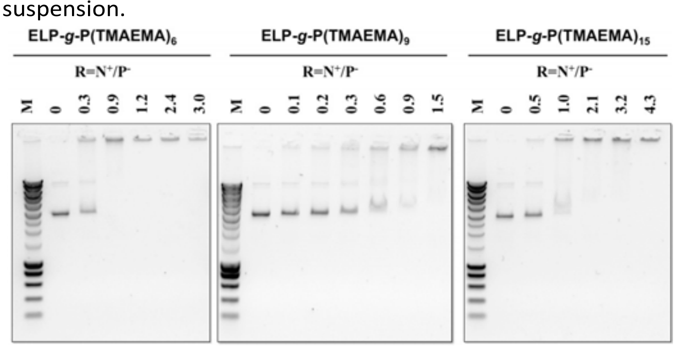

Fig. 6. Agarose gel electrophoresis assays showing the effect of N^+/P^- charge ratio for a) ELP-*g*-P(TMAEMA)$_6$, b) ELP-*g*-

http://dx.doi.org/10.1039/D0PY01293A

P(TMAEMA)$_9$ and c) ELP-*g*-P(TMAEMA)$_{15}$ on the electrophoretic mobility of linearized pUC19 plasmid (BamHI digested). M represents the molar masses of the marker (SmartLadder MW-1700-10 Eurogentec). C_{pDNA} = 0.095 mg/mL prepared in Tris 10 mM buffer at a pH=7.4, $C_{ELP\text{-}g\text{-}P(TMAEMA)6,9\ or15}$= 0.2 mg/mL prepared in water at pH = 6.0.

The ζ-potential reaches the values of +19±0.5, +21±1 and +24±0.5 mV for ELP-*g*-P(TMAEMA)$_6$, ELP-*g*-P(TMAEMA)$_9$ and ELP-*g*-P(TMAEMA)$_{15}$, respectively.

DNA-binding properties of chemoselectively modified ELPs bearing positively charged PTMAEMA oligomers were also evaluated through gel retardation experiments, which were carried on by analyzing the electrophoretic mobility of DNA (linearized pUC19 plasmid) at different charge ratios of DNA to hybrid cationic ELPs on an agarose gel (**Fig. 6**). Initial ELP can be used as negative control, showing that no DNA-binding affinity with the ELP was revealed at any ELP-to-plasmid amount reported in a mass/mass ratio, as previously observed in a recently published paper.[71] **Fig. 6a, 6b** and **6c** revealed that ELP-*g*-P(TMAEMA)$_6$, ELP-*g*-P(TMAEMA)$_9$ and ELP-*g*-P(TMAEMA)$_{15}$, respectively, were able to complex pDNA plasmid from a charge ratio N^+/P^- of around 1.0. pDNA/ELP-*g*-P(TMAEMA)$_X$ complexes can be then obtained from the interactions between cationic hybrid ELPs and nucleic acids following the stoichiometry of charges, *i.e,* N^+/P^- = 1.0, as well as complexes formed with ELPs bearing primary or secondary amine pendant groups at each methionine residue.[71]

pDNA/ELP-*g*-P(TMAEMA)$_X$ complexes characterization by AFM, TEM and DLS

Fig. 7a to 7f show AFM topographs of pDNA/ELP-*g*-P(TMAEMA)$_X$ complexes (with x=6, 9 and 15) prepared at the charge ratio N^+/P^- of 10. These positively charged complexes were prepared through the rapid one-shot mixing method by adding the specific amount of cationic hybrid ELPs to a negatively charged pDNA solution. From tapping mode AFM measurements it was observed that the structures of pDNA/ELP-*g*-P(TMAEMA)$_X$ complexes (with x=6,9 and 15) yield mainly globular shapes.[98-100] This was previously observed for complexes formed from electrostatic interactions between DNA and ELPs bearing primary or secondary amine pendant groups at each methionine residue, and the structure is similar for other polyplexes such as DNA/chitosan complexes.[98,100] **Table 3** summarizes pDNA/ELP-*g*-P(TMAEMA)$_X$ complex average particle sizes determined through AFM measurements, presenting an average of 115 ± 18 nm for the particle diameter (Particle distribution are shown in **Fig. S17**). This value is in the range of sizes between 100 and 200 nm, where the nuclear entry of complexes has been associated with the disappearance of the nuclear membrane during the cell division process.[101] Indeed, size is one of the important factors that have a significant role on transfection efficiency *in vivo*. Other known factors playing a role in complex stability are the polycation MW, local pH, charge ratio of polycation to DNA and the salt composition of the buffer.[71,78]

The TEM pictures obtained with pDNA/ELP-*g*-P(TMAEMA)$_X$ complexes (with x=6, 9 and 15) at a charge ratio N^+/P^- of 10 showed a major population of quasi-spherical nanoparticles with an average apparent diameter of 150 ± 18 nm (**Fig. 8a** to **c, Fig. S18**).

These quasi-spherical pDNA/ELP-*g*-P(TMAEMA)$_X$ cationic complexes are probably constituted by a neutral core surrounded by a cationic ELP-*g*-P(TMAEMA)$_X$ shell that warrants the colloidal stabilization.[97,102,103] Furthermore, hydrodynamic radius of the complexes formed at different charge ratios (5, 10 and 23) using the three ELP-*g*-P(TMAEMA)$_X$ synthesized were determined by DLS measurements. In good agreement with TEM measurements, DLS measurements showed complexes with a hydrodynamic diameter of 150 ± 10 nm. AFM results were found to be a little lower than DLS and TEM results, probably due to drying effects.

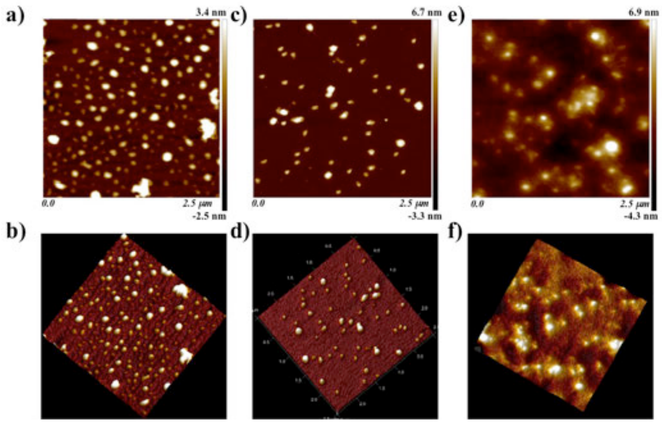

Fig. 7. AFM images of a), b) pDNA/ELP-*g*-P(TMAEMA)$_6$, c), d) pDNA /ELP-*g*-P(TMAEMA)$_9$ and e), f) pDNA /ELP-*g*-P(TMAEMA)$_{15}$ complexes prepared at the charge ratios N^+/P^- =10. C_{pDNA}= 0.03 mg/mL prepared in Tris 10 mM buffer at a pH=7.4 $C_{ELP\text{-}g\text{-}P(TMAEMA)6,\ 9\ or15}$= 0.2 mg/mL prepared in water at pH = 6.0.

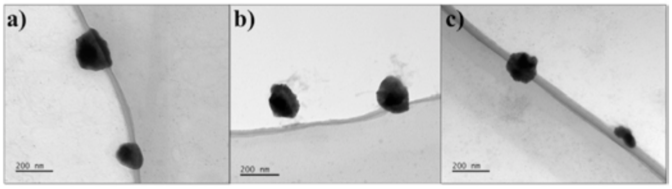

Fig. 8. TEM images of a) pDNA/ELP-*g*-P(TMAEMEA)$_6$, b) pDNA/ELP-*g*-P(TMAEMEA)$_9$ and c) pDNA/ELP-*g*-P(TMAEMEA)$_{15}$ complexes, prepared at a charge ratio N^+/P^-=10. C_{pDNz} = 0.03 mg/mL prepared in Tris 10 mM buffer at a pH=7.4, $C_{ELP\text{-}g\text{-}P(TMAEMA)6,9\ or15}$= 0.2 mg/mL prepared in water at pH = 6.0.

The use of this small nanometric complexes is crucial for effective *in vivo* delivery due to the physical constrains such as the dimensions of the capillary fenestrations, free diffusion through tissues and the elimination from the circulation by the

http://dx.doi.org/10.1039/D0PY01293A

reticuloendothelial system (RES), limiting the efficacy of large particles.[104,105]

Table 3 summarizes pDNA/ELP-*g*-P(TMAEMA)$_X$ complexes (with x = 6, 9 and 15) information determined through DLS measurements (hydrodynamic diameter, D_H and PDI) and ζ-potential measurements for three different charge ratios (5,10 and 23), and through TEM and AFM (average particle size) for the charge ratio of 10. As expected, the global charge (ζ-potential) of the cationic complexes obtained from electrophoretic mobility measurements remains constant at all N^+/P^- for a given pDNA/ELP-*g*-P(TMAEMA)$_X$, but increases proportionally with the increase of positive charges grafted to the ELP backbone.

Table 3. *pDNA/ELP-g-P(TMAEMA)$_x$ complexes characterization through Dynamic Light Scattering measurements (Hydrodynamic diameter, D_H, and PDI), AFM and TEM (average particle size), for three different charge ratios, N^+/P^-=5, 10 and 23. C_{pDNA} = 0.03 mg/mL prepared in Tris 10 mM buffer at a pH=7.4, $C_{ELP\text{-}g\text{-}P(TMAEMA)}$= 0.2 mg/mL prepared at pH = 6.0. pDNA/ELP-g-P(TMAEMA)$_x$ complexes were prepared through the rapid one-shot mixing method (cationic hybrid ELPs to anionic DNA).*

Complexes	DLS			ζ-potential (mV)	Particle diameter from AFM (nm) For R=10	Particle diameter from TEM (nm) For R=10
	Charge ratio (N^+/P^-)	D_H (nm)	PDI			
pDNA/ELP-g-P(TMAEMA)$_6$	5	148±5	0.218	+ 19±2	126±19	164±15
	10	130±4	0.232	+ 19±2		
	23	163±10	0.260	+ 19±2		
pDNA/ELP-g-P(TMAEMA)$_9$	5	180±10	0.220	+ 21±1	95±18	160±5
	10	130±2	0.220	+ 21±1		
	23	158±6	0.261	+ 21±1		
pDNA/ELP-g-P(TMAEMA)$_{15}$	5	145±15	0.225	+ 24±0.5	114±18	125±35
	10	115±2	0.219	+ 24±0.5		
	23	165±15	0.224	+ 24±0.5		

These results are consistent with the value of the plateau in the ζ-potential evolution as a function of the N^+/P^- ratio, corresponding to the excess of ELP-*g*-P(TMAEMA)$_X$ in the pDNA/ELP-*g*-P(TMAEMA)$_X$ complex suspension. Such an increase in global charge has been also observed for DNA/chitosan complexes, and was correlated to the degree of deacetylation (DDA) of the chitosans that led to higher charge densities.[106] *Huang et al.* also reported similar influences of DDA and MW on the ζ-potential of DNA/chitosan particles.[107]

Cationic hybrid ELP-*g*-P(TMAEMEA)$_{15}$ was selected as an example to evidence pDNA/cationic hybrid ELPs internalization in human cells. **Fig. 9a** shows the chemical structure of the pendant cationic oligomers P(TMAEMA)$_{15}$ grafted to each methionine residue of the native ELP. Cytometry analysis were performed in parallel with Laser Scanning Confocal Microscopy (LSCM) imaging to see whether labeled pDNA accumulated onto the cell surface, or if it penetrates into the cells after transfection. FITC-pDNA/ELP-*g*-P(TMAEMA)$_{15}$ complexes were prepared at three different charge ratios N^+/P^- (5, 10 and 23). As revealed through AFM and DLS measurements, FITC-labeled pDNA did not produce changes either in size or morphology of the complexes (**Fig. 9b** and **9c**).

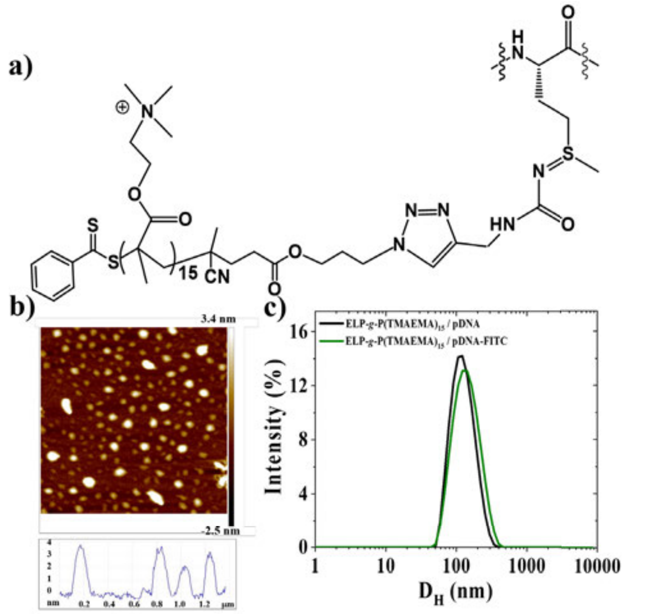

Fig. 9. a) Chemical structure of pendant cationic oligomer P(TMAEMA)$_{15}$ at each methionine residue of the native ELP, b) AFM images of FITC-pDNA/ELP-*g*-P(TMAEMA)$_{15}$ complexes prepared at the charge ratio N^+/P^- of 10. c) Intensity distribution from DLS measurements of pDNA/ELP-*g*-P(TMAEMA)$_{15}$ complexes prepared through rapid one-shot mixing of cationic hybrid ELPs to anionic unlabeled DNA (black) and to FITC-labeled pDNA (green). C_{pDNA}= 0.03 mg/mL prepared in Tris 10 mM buffer at a pH=7.4 $C_{ELP\text{-}g\text{-}P(TMAEMA)15}$= 0.2 mg/mL prepared in water at a pH= 6.

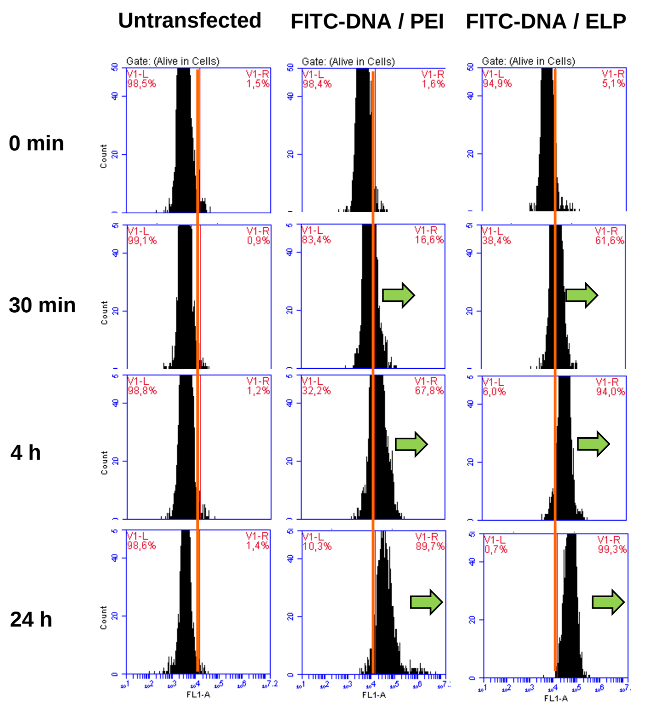

http://dx.doi.org/10.1039/D0PY01293A

Fig. 10. Cytometry analysis of cell fluorescence intensity. Mamalian HEK 293 cells were either untransfected, transfected with FITC-labeled pDNA/PEI complexes prepared at N^+/P^- ratio of 23, or transfected with FITC-labeled pDNA/ ELP-g-P(TMAEMA)$_{15}$ complexes prepared at charge ratio N^+/P^- of 23. Fluorescence intensity of cells was collected at 0 min, 30 min, 4 hours and 24 hours post-transfection. FITC was excited with a 488 nm laser and fluorescence was acquired on FL1 channel (533/30 nm).

Biological test

To evaluate the efficiency of DNA transfection using the cationic ELPs, human HEK 293 cells were incubated with complexes of FITC-labeled plasmid DNA and ELP-*g*-P(TMAEMA)$_{15}$. Cell fluorescence was analyzed over time to follow the incorporation of FITC-pDNA as depicted in **Fig. 10**. After 30 min of incubation we can observe a global increase of the cell population fluorescence (histogram shift to the right, **Fig. 10**).

This shift increased up to 24 hours post-transfection. At this time point, the cell population fluorescence was about one order of magnitude higher than that measured before transfection, or measured in the control experiment after 24 hours of incubation, where no transfection agent was added (left column, **Fig. 10**). A similar trend was observed when PEI, the positive control, was used as transfection agent. No further increase in the cell population fluorescence was observed between 24 hours and 48 hours post-transfection (data not shown). In order to know whether the labeled pDNA accumulated onto the cell surface, or entered into the cells, Laser Scanning Confocal Microscopy (LSCM) was performed (**Fig. 11**).

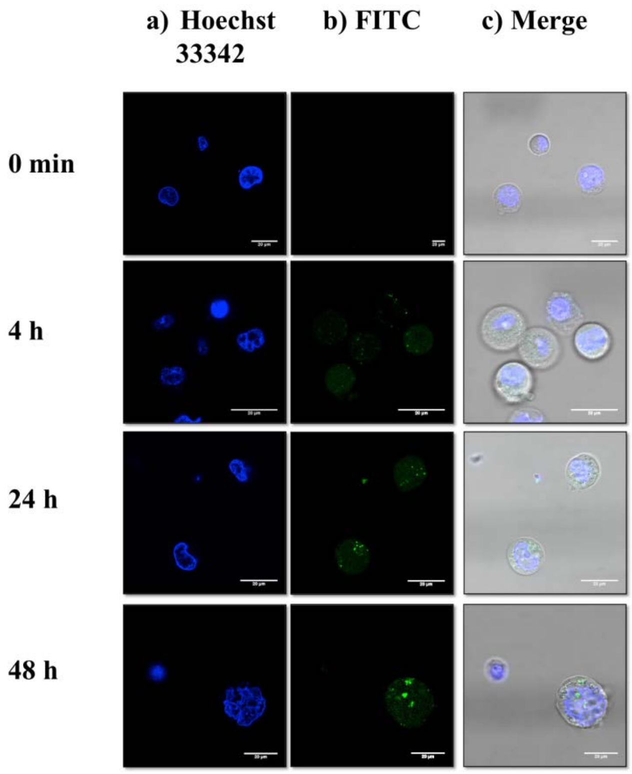

Fig. 11. Laser scanning confocal microscopy images of cells after different post-transfection time. Cell nuclei were stained with Hoechst 33342 (blue) and pDNA was labeled with FITC (green). Fluorescence microscopy images of cells were captured at 0 min, 4 hours, 24 hours and 48 hours post-transfection in the a) blue channel, b) green channel and c) merged.

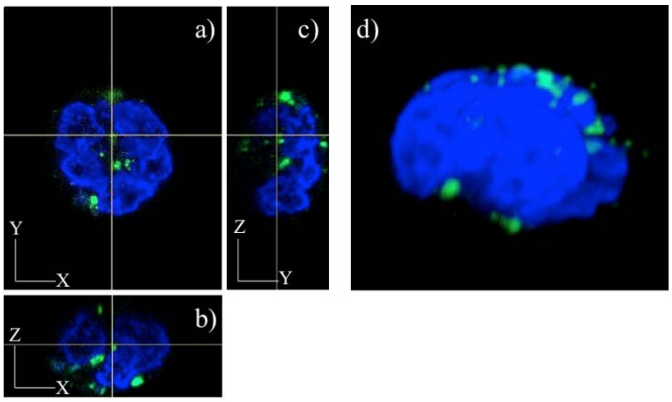

Fig. 12. a) A single z-slice of the cell surface is represented on the X-Y plane from a Z-projection of 60 optical sections with a step size of 0.7 µm. Then, orthogonal projections were generated from X-Y image on the X-Z (b) and Y-Z (c) planes along directions defined by the white lines. d) 3D visualization of a typical cell at 48 hours post-transfection.

http://dx.doi.org/10.1039/D0PY01293A

As depicted on **Fig. 11**, after 4 hours of transfection the fluorescence was evenly distributed, suggesting that the plasmid was on the cell surface. At later times, intense spots of FITC-Labeled DNA appeared inside the cells, most probably located into organelles that might be endosomes or lysosomes. Indeed, 3D analysis of a typical cell at 48 hours post-transfection clearly showed that fluorescent elements were internalized into cells, close to the nucleus (**Fig. 12**, **Video S1**). These results suggest that cationic ELPs are efficient to promote mammalian cell transfection by pDNA. Further investigations should be performed to explore the capacity of this class of polymer to deliver other kind of nucleic acids, such as RNA.

Conclusions

For the first time, low DPs for PTMAEMA were achieved through RAFT polymerization using an azide containing chain transfer agent, to provide cationic oligomers with relatively low DPs, *i.e.* $15 \geq DP \geq 6$. These oligomers were successfully clicked onto ELPs to provide them a cationic character, and give them the ability to complex nucleic acids. The different cationic PTMAEMA oligomers were analyzed through SEC measurements and ^{1}H NMR, from which it was possible to determine a narrow polydispersity index (between 1.15 and 1.20), and observe that the molar masses increased proportionally to the calculated DP.

ELPs were chemically functionalized by modification of the thioether group of each methionine residue using an alkyne-containing oxaziridine derivatives and PTMAEMA cationic oligomers were grafted by copper catalyzed azide-alkyne cycloaddition to provide positive charges along the ELP chain in a controlled manner. This approach allows accurate control over the number of positive charges provided to the native ELP and precise determination of the stoichiometry during pDNA/ELP-*g*-(PTMAEMA)$_x$ complex formation. The average molar masses (MW) of ELPs derivatives were determined using the *dn/dc* method from SEC measurements, resulting in molar mass values close to those estimated through ^{1}H NMR measurements.

The formation of an electrostatic complex from the addition of positively charged ELP-*g*-P(TMAEMA)$_X$ into a dilute pDNA solution was evidenced through gel retardation, ζ-potential, TEM, AFM and DLS measurements. From ζ-potential measurements it was found that electrostatic interactions between ELP-*g*-(PTMAEMA)$_x$ and pDNA take place in the solution and are responsible of the complexation process of pDNA. Results were analyzed in terms of the NH_3^+ amount added to a pDNA solution, expressed as N^+/P^-. At ζ-potential > 0 mV, a plateau corresponding to an excess of ELP-*g*-P(TMAEMA)$_X$ in the pDNA/ELP-*g*-P(TMAEMA)$_X$ complex suspension was obtained for the three ELP derivatives synthetized. The ζ-potential values reached at the plateau were +19 ± 0.5, +21 ± 1 and +24 ± 0.5 mV for ELP-*g*-P(TMAEMA)$_6$, ELP-*g*-P(TMAEMA)$_9$ and ELP-*g*-P(TMAEMA)$_{15}$, respectively. Electrophoretic mobility of pDNA at different charge ratios of pDNA to hybrid cationic ELPs were performed on agarose gels, and revealed that the three ELP-g-P(TMAEMA)$_x$ (with x = 6,9 and 15) were able to complex pDNA at a charge ratio N^+/P^- of 1.0, in a way similar to the complexes formed with ELPs bearing primary or secondary amine pendant groups at each methionine residue.[71]

pDNA/ELP-*g*-P(TMAEMA)$_X$ (with x= 6,9 and 15) stable nanoparticles, both in size and charge, were obtained in excess of positive charges (N^+/P^- >1). We report here the D_H and PDI (DLS), the average particle size (TEM and AFM), as well as the net charge (ζ-potential measurements) for charge ratios N^+/P^- of 5, 10 and 23. Dynamic light scattering measurements revealed an average particle size of around 150 ± 10 nm. pDNA/ELP-*g*-P(TMAEMA)$_{15}$ complex morphology and sizes were also studied through AFM measurements, from which it was possible to identify that the structures of the obtained polyplexes mainly yield globular shapes. From TEM measurements, the morphology of pDNA/ELP-g-P(TMAEMA)$_{15}$ nanoparticles, prepared at a charge ratio N^+/P^- of 10, was found to be mainly quasi-spherical with an average apparent diameter around 150 ± 18 nm.

Cytometry analyses were achieved in parallel with Laser Scanning Confocal Microscopy (LSCM) imaging to decipher whether labeled pDNA was accumulated on human cell surface or integrated in cells after transfection. pDNA/ELP-*g*-P(TMAEMEA)$_{15}$ complexes were prepared at different charge ratios N^+/P^- (5, 10 and 23) and were used as an example to evidence internalization in human cells. The obtained results suggest that cationic hybrids ELP-*g*-P(TMAEMEA)$_X$ are efficient agents to promote mammalian cell transfection of DNA. Further investigations should be performed to explore applicability to cell transfer of other nucleic acids material like RNA.

Conflicts of interest

"There are no conflicts to declare".

Acknowledgements

L.M. Bravo-Anaya acknowledges the fellowship grant given by CONACYT (CVU 350759). The help of Marie Rosselin for NMR analyses is particularly acknowledged.

The help of Guillaume Goudounet for ELP production is particularly acknowledged. We acknowledge Graeme Moad (CSIRO) and Steve Armes (University of Sheffield) for fruitful discussions. Electron microscopy was performed at Bordeaux Imaging Center, a service unit of the CNRS-INSERM and Bordeaux University, member of the national infrastructure France BioImaging. Campus-B project, CNRS, Univ. Bordeaux, Bordeaux INP and the Région Nouvelle Aquitaine are also acknowledged. This work was also supported by the French National Research Agency (ANR-15-CE07-0002) and the Cancéropole Grand Sud-Ouest (Emergence 2018-E18).

References

http://dx.doi.org/10.1039/D0PY01293A

1 I. Cobo, M. Li, B. S. Sumerlin and S. Perrier, *Nat. Mater.*, 2015, **14**, 143.
2 J. P. Magnusson, A. O. Saeed, F. Fernandez-Trillo and C. Alexander, *Polym. Chem.*, 2011, **2**, 48.
3 S. Kango, S. Kalia, P. Thakur, B. Kumari and D. Pathania, in Advances in Polymer Science, Springer, 2014, vol. 267, pp.283-311.
4 Q. Xie, J. Pan, C. Ma, G. Zhang, *Soft Matter*, 2019, **15**, 1087.
5 Y. Lu, A. A. Aimetti, R. Langer and Z. Gu, *Nat. Rev. Mater.,* 2017, **2**, 1.
6 I. Stanislawska, W. Liwinska, M. Lyp, Z. Stojek and E. Zabost, *Molecules*, 2019, **24**, 1.
7 A. Marya; N. Ravin, *Prog. Polym. Sci.*, 2013, 38, 767.
8 D. Witzigmann, D. Wu, S.H. Schenk, V. Balasubramanian, W. Meier and J. Huwyler, *ACS Appl. Mater. Interfaces,* 2015, **19**, 10446.
9 A. Ghadban, E. Reynaud, M. Rinaudo and L. Albertin, *Polym. Chem.,* 2013, **4**, 4578.
10 G. Sen, A. Sharon and S. Pal, in Biopolymers: Biomedical and Environmental Applications, Scivener Publishing, 2011, vol. 5, pp. 99–127.
11 D. W. P. M. Loewik, L. Ayres, J. M. Smeenk and H. J. C. M. Van, *Adv. Polym. Sci.,* 2006, **202**, 19.
12 J. M. Smeenk, D. W. P. M. Loewik, J. C. M. van Hest, *Curr. Org. Chem.,* 2005, **9**, 1115.
13 C. Schatz, S. Lecommandoux, Macromol. *Rapid Commun.*, 2010, **31**, 1664.
14 N. Sanoj Rejinold, P. R. Sreerekha, K. P. Chennazhi, S. V. Nair and R. Jayakumar, *Int. J. Biol. Macromol.,* 2011, **49**, 161.
15 W. M. Argüelles-Monal, J. Lizardi-Mendoza, D. Fernández-Quiroz, M. T. Recillas-Mota and M. Montiel-Herrera, *Polymers,* 2018, **10**, 1.
16 F. E. Alemdaroglu and A. Herrmann, *Org. Biomol. Chem.*, 2007, **5**, 1311.
17 F. E. Alemdaroglu, J. Wang, M. Börsch, R. Berger and A. Herrmann, *Angew. Chem. Int. Ed.,* 2008, **47**, 974.
18 J. M. Smeenk, D. W. P. M. Löwik and J. C. M. van Hest, *Curr. Org. Chem.,* 2005**, 9,** 1115.
19 A. Rosler, H. A. Klok, I. W. Hamley, V. Castelletto and O. O. Mykhaylyk, *Biomacromolecules*, 2003, **4**, 859.
20 J. M. Smeenk, M. B. J. Otten, J. Thies, D. A. Tirrell, H. G. Stunnenberg, J. C. M. van Hest, *Angew. Chem. Int., Ed.,* 2005, **44**, 1968.
21 D. W. P. M. Löwik, L. Ayres, J. M. Smeenk and J. C. M. Van Hest, *Adv. Polym. Sci.,* 2006, **202**, 19.
22 J.C. Rodríguez-Cabello, L. Martín, M. Alonso, F. J. Arias and A.M. Testera, *Polymer* 2009, **50**, 5159.
23 F. C. M. Smits, B. C. Buddingh, M. B. Van Eldijk and J. C. M. Van Hest, *Macromol. Biosci.,* 2015, **15**, 36.
24 R. Petitdemange, E. Garanger, L. Bataille, W. Dieryck, K. Bathany, B. Garbay, T. J. Deming and S. Lecommandoux, *Biomacromolecules*, 2017, **18**, 544.
25 J. R. Kramer, R. Petitdemange, L. Bataille, K. Bathany, A.-L. Wirotius, B. Garbay, T. J. Deming, E. Garanger and S. Lecommandoux, *ACS Macro Lett.,* 2015, **4**, 1283.
26 D. E. Meyer and A. Chilkoti, *Biomacromolecules*, 2004, **5**, 846.
27 T. Kowalczyk, K. Hnatuszko-Konka, A. Gerszberg and A. K. Kononowicz, *World J. Microbiol. Biotechnol.,* 2014, **30**, 2141.
28 J.R. McDaniel, D.C. Radford and A. Chilkoti, *Biomacromolecules*, 2013, **14**, 2866.
29 J. A. MacKay, D. J. Callahan, K. N. FitzGerald and A. Chilkoti, *Biomacromolecules*, 2010, **11**, 2873.
30 D. W. Urry, M. M. Long, B. A. Cox, T. Ohnishi, L. W. Mitchell, M. Jacobs, *Biochim. Biophys. Acta, Protein Struct.,* 1974, **371**, 597.
31 C. H. Luan, R. D. Harris, K. U. Prasad and D. W. Urry, *Biopolymers*, 1990, **29**, 1699.
32 D. E. Meyer and A. Chilkoti, *Biomacromolecules*, 2004, **5**, 846.
33 L.M. Bravo-Anaya, R. Petitdemange, M. Rosselin, E. Ibarboure, B. Garbay, E. Garanger, T. J. Deming, S. Lecommandoux, *Biomacromolecules*, 2020, XXX, XXX.
34 R. Petitdemange, E. Garanger, L. Bataille, K. Bathany, B. Garbay, T. J. Deming and S. Lecommandoux, *Bioconjugate Chem.,* 2017, **28**, 1403.
35 A. J. Simnick, D. W. Lim, D. Chow and A. Chilkoti, *Polym. Rev.,* 2007, **47**, 121.
36 J. R. McDaniel, J. Bhattacharyya, K. B. Vargo, W. Hassouneh, D. Hammer and A. Chilkoti, *Angew. Chem., Int. Ed.,* 2013, **52**, 1683.
37 M. R. Dreher, D. Raucher, N. Balu, O. M. Colvin, S. M. Ludeman and A. Chilkoti, *J. Controlled Release,* 2003, **91**, 31.
38 R. Saxena and M. Nanjan, *J. Drug Delivery*, 2015, **22**, 156.
39 W. Hassouneh, S.R. MacEwan and A. Chilkoti, *Methods Enzymol.,* 2012, **502**, 215.
40 S. Fluegel, J. Buehler, K. Fischer, J. R. McDaniel, A. Chilkoti and M. Schmidt, *Chemistry*, 2011, **17**, 5503.
41 Y, Xiao, Z, S. Chinoy, G, Pecastaings, K. Bathany, E. Garanger and S. Lecommandoux, *Biomacromolecules*, 2020, **21**, 114.
42 G. Le Fer, D. Portes, G. Goudounet, J-M. Guigner, E. Garanger and S. Lecommandoux, *Org. Biomol. Chem.,* 2017, **15**, 10095.
43 L. Ayres, M. R. J. Vos, P. J. H. M. Adams, I.O. Shklyarevskiy and J.C.M. van Hest, *Macromolecules*, 2003, **36**, 5967.
44 L. Ayres, K. Koch, P. J. H. M. Adams and J. C. M. van Hest, *Macromolecules*, 2005, **38**, 1699.
45 R. M. Conrad and R. H. Grubbs, Angew. *Chem. Int. Edit.,* 2009, **48**, 8328.
46 S. K. Roberts, A. Chilkoti and L. A. Setton, *Biomacromolecules*, 2007, **8**, 2618.
47 W. Gao, D. Xu, D. W. Lim, S. L. Craig and A. Chilkoti, *Polym. Chem.,* 2011, **2**, 1561.
48 F. Fernández-Trillo, A. Duréault, J. P. M. Bayley, J. C. M. van Hest, J. C. Thies, T. Michon, R. Weberskirch and N. R. Cameron, *Macromolecules*, 2007, **40**, 6094.
49 X. Ge, D. S. C. Yang, K. Trabbic-Carlson, B. Kim, A. Chilkoti and C. D. M. Filipe, *J. Am. Chem. Soc.,* 2005, **127**, 11228.
50 D. Weller, J. R. McDaniel, K. Fischer, A. Chilkoti and M. Schmidt, *Macromolecules*, 2013, **46**, 4966.
51 D. A. Shipp, *Polym. Rev.,* 2011, **51**, 99.
52 J.-S. Wang and K. Matyjaszewski, *J. Am. Chem. Soc.,* 1995, **117**, 5614.
53 M. Kato, M. Kamigaito, M. Sawamoto and T. Higashimura, *Macromolecules*, 1995, **28**, 1721.
54 J. Chiefari, Y. K. Chong, F. Ercole, J. Kristina, J. Jeffery, T. P. T. Le, R. T. A. Mayadunne, G. F. Meijs, C. L. Moad, G. Moad, E. Rizzardo and S. H. Thang, *Macromolecules*, 1998, **31**, 5559.
55 C. Chen, F. Kong, X. Wei and S. H. Thang, *Chem. Commun.,* 2017, **53**, 10776.
56 C. Boyer, V. Bulmus, T. P. Davis, V. Ladmiral and J. Liu, S. Perrier, *Chem. Rev.,* 2009, **109**, 5402.
57 *F. J. Xu, K. G. Neoh and E. T. Kang, Prog*. Polym. Sci., 2009, **34**, 719.
58 M. Ahmed and R. Narain, *Prog. Polym. Sci.,* 2013, **38**, 767.
59 S. M. Perrier, *Nat. Chem.,* 2010, **2**, 811.
60 V. Bulmus, Polym Chem., 2011, 2, 1463.
61 G. Moad, E. Rizzardo and H. Thang*, Chem. Asian J.,* 2013, **8**, 1634.
62 J. Hentschel, K. Bleek, O. Ernst, J-F. Lutz, G. H. Borner, *Macromolecules*, 2008, **41**,1073.
63 H. Willock and R. K. O'Reilly, *Polym. Chem.,* 2010, **1**, 149.
64 T. J. Thoms, H.-A. Tajmir-Riahi and C. K. S. Pillai, *Molecules*, 2019, **24**, 3744, 1.
65 C. J. Needham, A. K. Williams, S. A. Chew, F. K. Kasper, A. G. Mikos, *Biomacromolecules*, 2012, **13**, 1429.

http://dx.doi.org/10.1039/D0PY01293A

66 B. Santos-Carballal, E. Fernández Fernández and F. M. Goycoolea, *Polymers*, 2018, **10**, 444.
67 I. Honoré, S. Grosse, N. Frison, F. Favatier, M. Monsigny and I. Fajac, *J. Controll. Release*, 2005, **107**, 537.
68 L. M. P. Vermeulen, S. C. De Smedt, K. Remaut and K. Braeckmans, *Eur. J. Pharm. Biopharm.,* 2018, **129**, 184.
69 R. V. Benjaminsen, M. A. Mattebjerg, J. R. Henriksen, S. M. Moghini and T. L. Andresen, *Mol. Ther.,* 2013, **21**, 149.
70 M. K. Lee, S. K. Chun, W. J. Choi, J. K. Kim, S. H. Choi, A. K. Kim, K. Oungbho, J. S. Park, W. S. Ahn and C. K. Kim, *Biomaterials*, 2005, **26**, 2147.
71 L. M. Bravo-Anaya, B. Garbay, J. L. E. Nando-Rodriguez, F. Carvajal Ramos, E. Ibarboure, K. Bathany, Y. Xia, J. Rosselgong, G. Joucla, E. Garanger and S. Lecommandoux, *J.Colloid Interf. Sci.,* 2019, **557**, 777.
72 M. Rosselin, Y. Xiao, L. Belhomme and S. Lecommandoux, E. Garanger, *ACS Macro Lett.,* 2019, **8**, 1648.
73 D. Quemener, T. P. Davis, C. Barner-Kowollik and M. H. Stenzel, *Chem. Commun.* 2006, **48**, 5051.
74 J. Cavanagh, W. J. Fairbrother, A. G. Palmer and N. J. Skelton, in Protein NMR Spectroscopy: Principles and Practice, Academic Press, San Diego, CA, 1995.
75 K. Wüthrich, in NMR of Proteins and Nucleic Acids, John Wiley & Sons, 1986.
76 A. D. Kulkarni, Y. H. Vanjari, K. H. Sancheti, H. M. Patel, V. S. Belgamwar, S. J. Surana and C. V. Pardeshi, *Nanomed. Biotechnol.,* 2016, **44**, 1615.
77 C. Schatz, J. Lucas, C. Viton, A. Domard, C. Pichot and T. Delair, *Langmuir*, 2004, **20**, 7766.
78 L. M. Bravo-Anaya, K. G. Fernandez-Solis, J. Rosselgong, J. L. E. Nano-Rodriguez, F. Carvajal, M. Rinaudo, *Int. J. Biol. Macromol.,* 2019, **126**, 1037.
79 F. Yang, W. Wu, S. Chen and W. Gan, *Soft Matt.,* 2017, **13**, 638.
80 L. Xu, F. Mallamace, Z. Yan, F. W. Starr, S. V. Buldyrev and H. E. Stanley, *Nat. Phys.,* 2009, **5**, 565.
81 T. Ishii, Y. Okahata and T. Sato, *Chem. Lett.,* 2000, **4**, 386.
82 M. De Los Milagros Bassani Molinas, C. Beer, F. Hesse, M. Wirth and R. Wagner, *Cytotechnology*, 2014, **66**, 493.
83 J. Rosselgong, S. P. Armes, W. R. S. Barton and D. Price, *Macromolecules*, 2010, **43**, 2145.
84 S. Perrier, *Macromolecules*, 2017, **50**, 7433.
85 M.J. Derry, L.A. Fielding, N.J. Warren, C.J. Mable, A.J. Smith, O.O. Mykhaylyk and S.P. Armes, *Chemical Science,* 2016, **7**(8), 5078.
86 P.K. Das, D.N. Dean, A.L. Fogel, F. Liu, B.A. Abel, C.L. McCormick, E. Kharlampieva, V. Rangachari and S.E. Morgan, *Biomacromolecules*, 2017, **18**, 3359.
87 E.F. Palermo and K. Kuroda, *Biomacromolecules*, 2009, **10**, 1416.
88 Y.-L. Lin, G. Jiang, L.K. Birrell and M.E.H. El-Sayed , *Biomaterials*, 2010, **31**, 7150.
89 H.-Y. Yu, J. Huang, P.R. Chang, in Cellulose-Based Graft Copolymers, 2015.
90 L.M. Bravo-Anaya, J.F.A. Soltero, M. Rinaudo and *Int. J. Biol. Macromolecules,* 2016, **88**, 345.
91 A. Sillero and J. Maireles Ribeiro, *Anal. Biochem.,* 1989, **179**, 319.
92 J.-P. Clamme, G. Krishnamoorthy and Y. Mély, *Biochim Biophys Acta.,* 2003, **1617**, 52.
93 S.N. Uddin and K.K. Islam, *Trends in Medical Research*, 2006, **1**, 86.
94 Q. Gan, T. Wang, C. Cochrane and P. McCarron, *Colloids Surf. B*, 2005, **44**, 65.
95 I. Serrano-Sevilla, A. Artiga, S.G. Mitchell, L. De Matteis and J.M. de la Fuente, *Molecules*, 2019, **24**, 1.
96 H. Ragelle, G. Vandermeulen and V. Préat, J. *Control. Release,* 2013, **172**, 207.
97 C. Schatz, A. Domard, C. Viton, C. Pichot, T. Delair, *Biomacromolecules*, 2004, **5**, 1882.
98 M. Alatorre-Meda, P. Taboada, F. Hartl, T. Wagner, M. Freis and J.R. Rodríguez, *Colloids Surf. B,* 2011, **82**, 54.
99 F. Amaduzzi, F. Bomboi, A. Bonincontro, F. Bordi, S. Casciardi, L. Chronopoulou, M. Diociaiuti, F. Mura, C. Palocci and S. Sennato, *Colloid Surf. B*, 2014, **114**, 1.
100 S. Danielsen, G. Maurstad and B.T. Stokke, *Biopolymers*, 2005, **77**, 86.
101 K. Miyata, N. Nishiyama and K. Kataoka, *Chem. Soc. Rev.,* 2012, **41**, 2562.
102 T. Delair, *Eur. J. Pharm. Biopharm.,* 2011, **78**, 10.
103 D. Wu and T. Delair, *Carbohydr. Polym.,* 2015, **119**, 149.
104 D. Pezzoli, E. Giupponi, D. Mantovani and G. Candiani, *Sci Rep.,* 2017, **8**, 1.
105 W. Li and F.C. Jr. Szoka, *Pharm. Res.,* 2007, **24**, 438.
106 M. Lavertu, S. Méthot, N. Tran-Khanh and M.D. Buschmann, *Biomaterials*, 2006, **27**, 4815.
107 M. Huang, C.W. Fong, E. Khor, L.Y. Lim, Transfection efficiency of chitosan vectors: effect of polymer molecular weight and degree of deacetylation, *J. Control. Release*, 2005, **106(3),** 391-406.

http://dx.doi.org/10.1039/D0PY01293A

Supporting Information for Polymer Chemistry manuscript

Coupling of RAFT Polymerization and Chemoselective Post-modifications of Elastin-like Polypeptides for the Synthesis of Gene Delivery Hybrid Vectors

L. M. Bravo-Anaya,[1*] J. Rosselgong,[1*] K. G. Fernández,[1,2,] Y. Xiao,[1] A. Vax,[1] E. Ibarboure,[1] A. Ruban,[1] C. Lebleu,[1] G. Joucla,[3] B. Garbay,[1] E. Garanger,[1] and S. Lecommandoux[1]

[1] University of Bordeaux, CNRS, Bordeaux INP, LCPO, UMR 5629, F-33600, Pessac, France.

[2] Centro Universitario UTEG, Departamento de Investigación, Héroes Ferrocarrileros #1325 C.P. 44460, Guadalajara, Jalisco, México.

[3] University of Bordeaux, CNRS, Bordeaux INP, CBMN, UMR 5248, F-33615, Pessac, France.

Synthesis of azido-RAFT agent

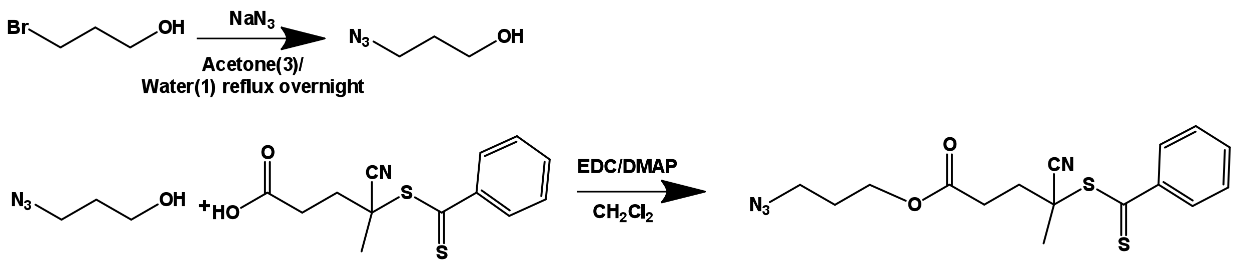

Scheme S1.- Synthesis of the azido-RAFT agent [1].

3-bromo-1-propanol (15.0 g, 1 eq, 108 mmol) and sodium azide (12.3 g, 1.75 eq, 189 mmol) were dissolved in a mixture of acetone (180 mL) and water (60 mL) and the resulting solution was refluxed overnight. Acetone was then removed under reduced pressure, 100 mL of water were added and the mixture was extracted with diethyl ether (3 x 100 mL). The organic layers collected were dried over $MgSO_4$ and, after removal of the solvent under reduced pressure; 3-azido-1-propanol was isolated as colorless oil (8.32 g, 76%).

A solution of (4-cyanopentanoic acid)-4-dithiobenzoate (3.26 g, 1 eq, 11.6 mmol) and 3-azido-1-propanol (5.90 g, 5 eq, 17 mmol) in dichloromethane (200 mL) was cooled to 0 ºC and *N*-(3-dimethylaminopropyl)-N'ethylcarbodiimide hydrochloride (6.71 g, 3 eq, 35.0 mmol) and 4-dimethylaminopyridine (71.2 mg, 0.05 eq, 0.58 mmol) were subsequently added. The orange solution was stirred at 0 ºC for 2h, then at ambient temperature overnight. The reaction mixture was washed with water (2x200mL) and dried over $MgSO_4$. The volatiles were removed under reduced pressure and the crude product purified by flash chromatography (SiO_2, 1) 100% CH_2Cl_2; 2) Hexane/Ethyl acetate 4/1) (2.81 g, 67%). Figure S1 represents step by step the procedure to obtain the azido-RAFT agent followed by ^{1}H NMR.

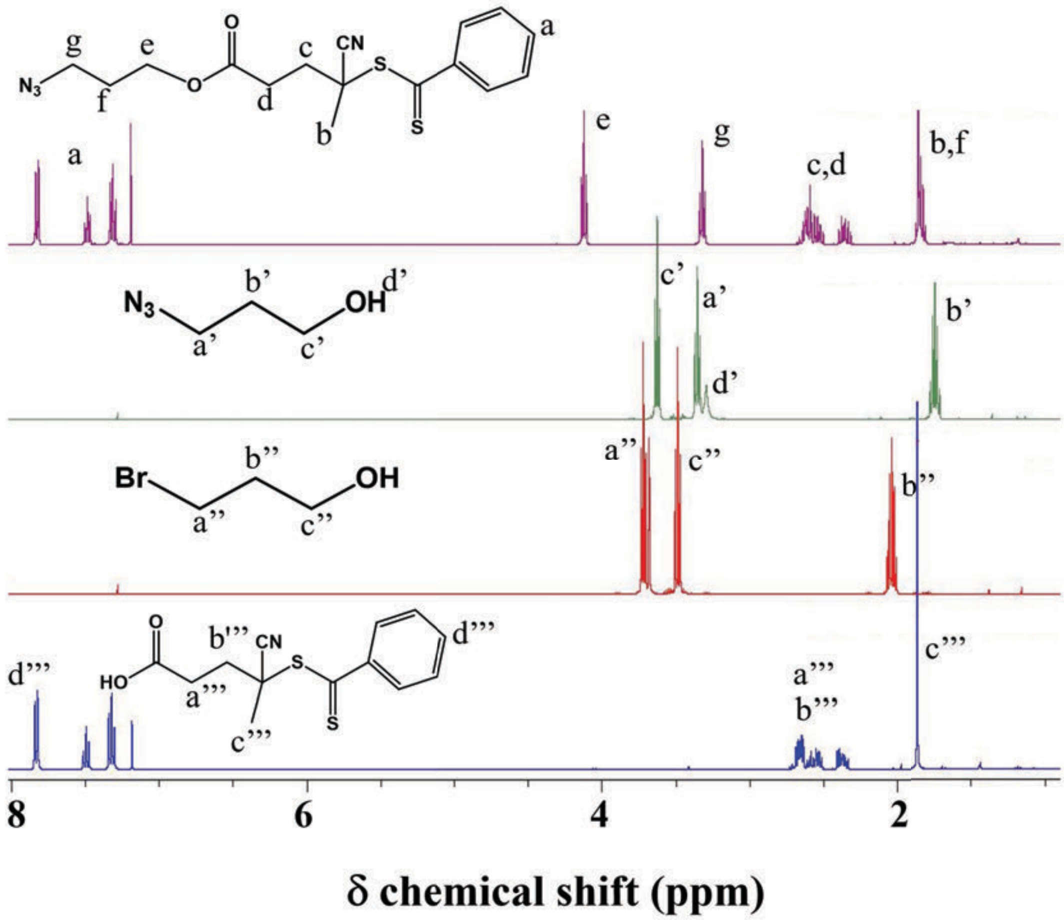

Figure S1.- ^{1}H-NMR spectrum of azido-RAFT agent and its precursors in $CDCl_3$ 25 °C, 400.2 MHz).

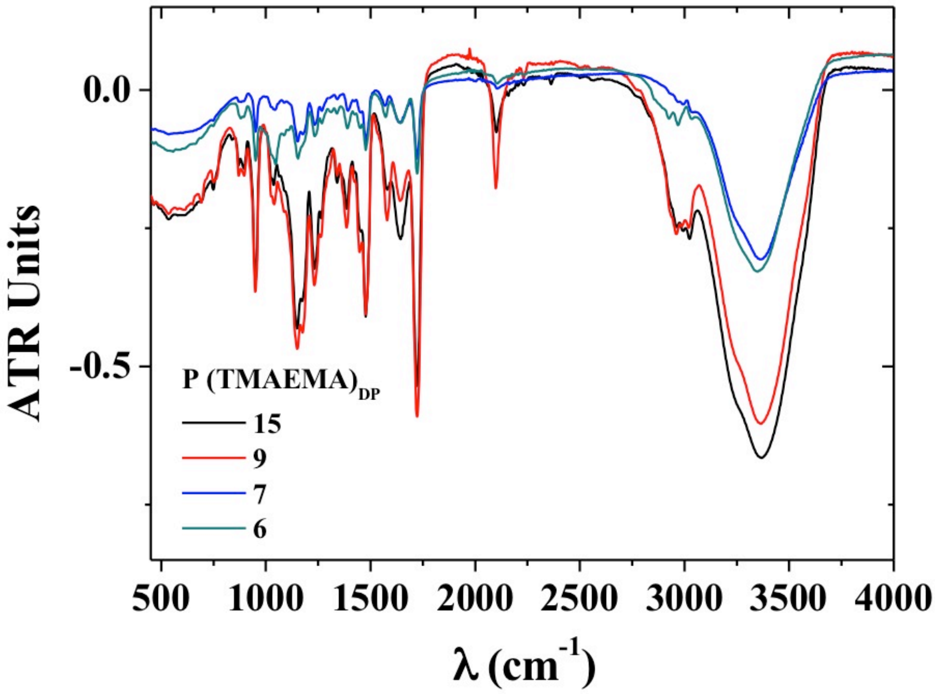

Figure S2.- Infra-red spectrum of P(TMAEMA)$_{DP}$ oligomers, DP = 15, 9, 7, 6.

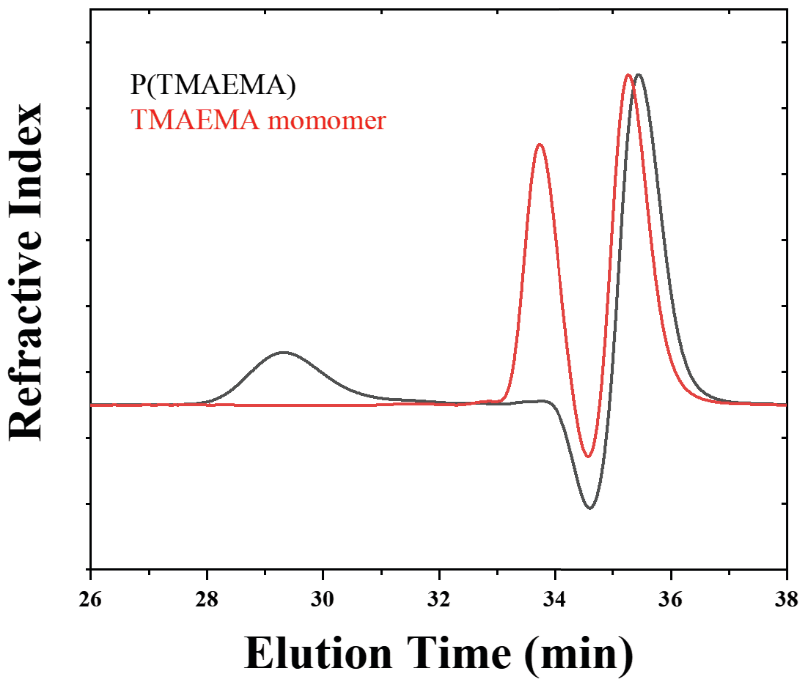

Figure S3.- SEC traces in AcOH/Ammonium Acetate/ACN of P(TMAEMA)$_{15}$ and the TMAEMA monomer using a RI detector.

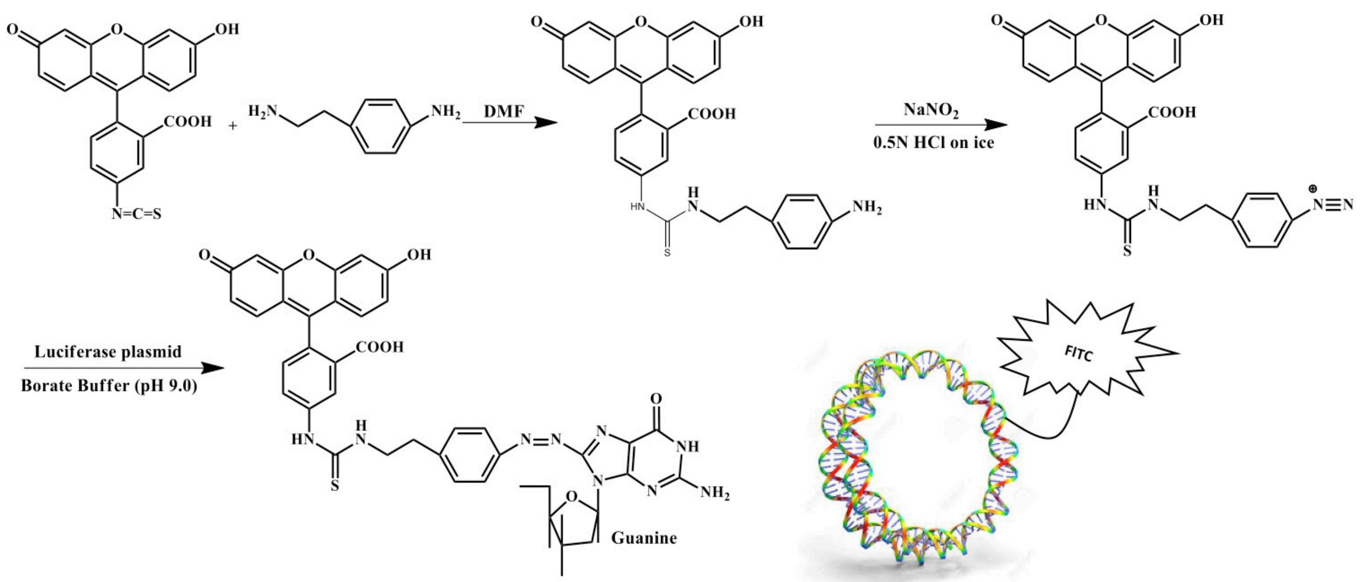

Scheme S2.- Synthesis of the fluorescent plasmid, pDNA-FTIC. Reproduced from [2] with permission.

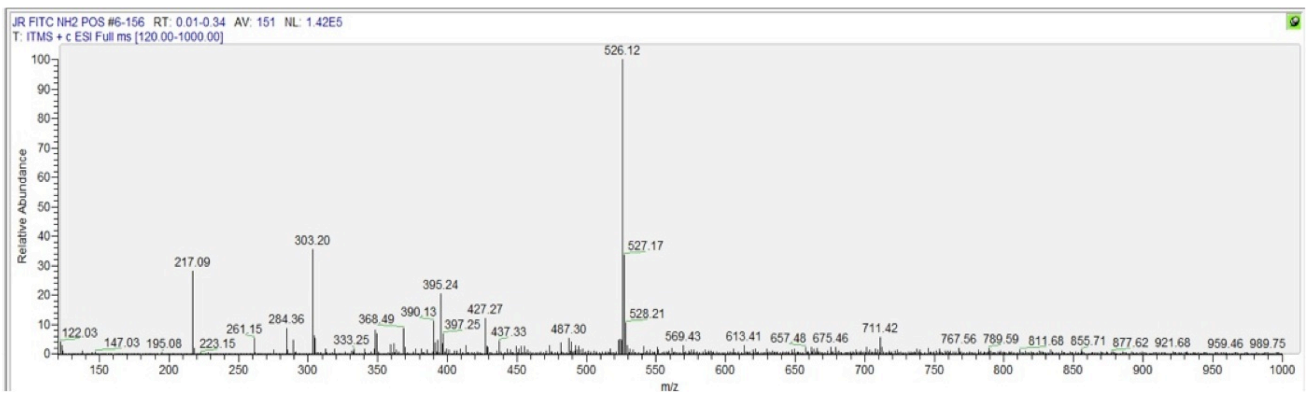

Figure S4. – Mass spectroscopy spectra of the pDNA-FITC intermediate.

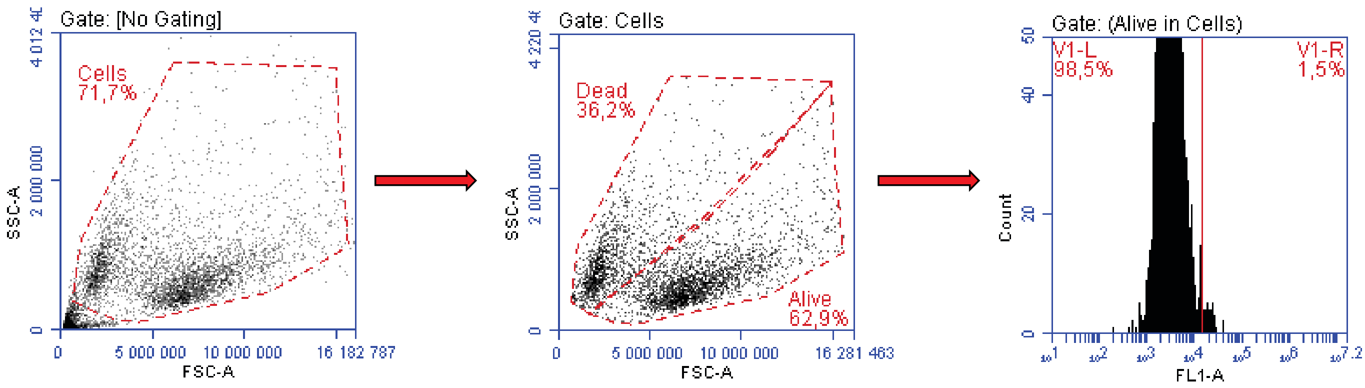

Figure S5.- Processing procedure of the cytometry events. On the negative control assay (untransfected cells) the population of cells was selected in order to discard small debris and artefacts. Thereafter two gates were defined to sort “Alive” or “Dead” cells. Finally the “Alive” gated cells were analyzed according to their fluorescence intensity. The negative control sample was the reference to set limit for non-fluorescent cells (left hand) or fluorescent cells (right hand). Gates and limits defined on negative control sample were applied for all samples.

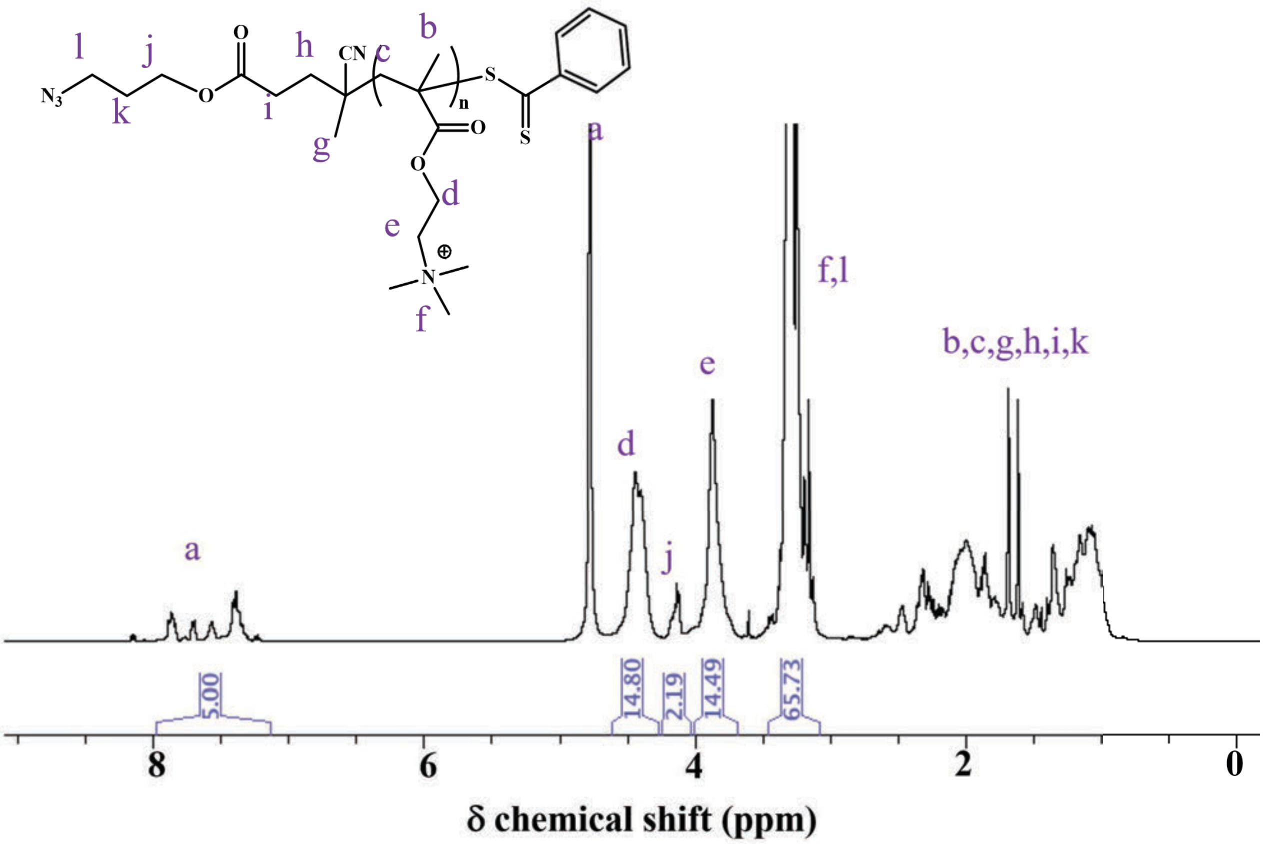

Figure S6. ^{1}H NMR spectrum of the $P(TMAEMA)_7$ in D_2O (25 °C, 400.2 MHz).

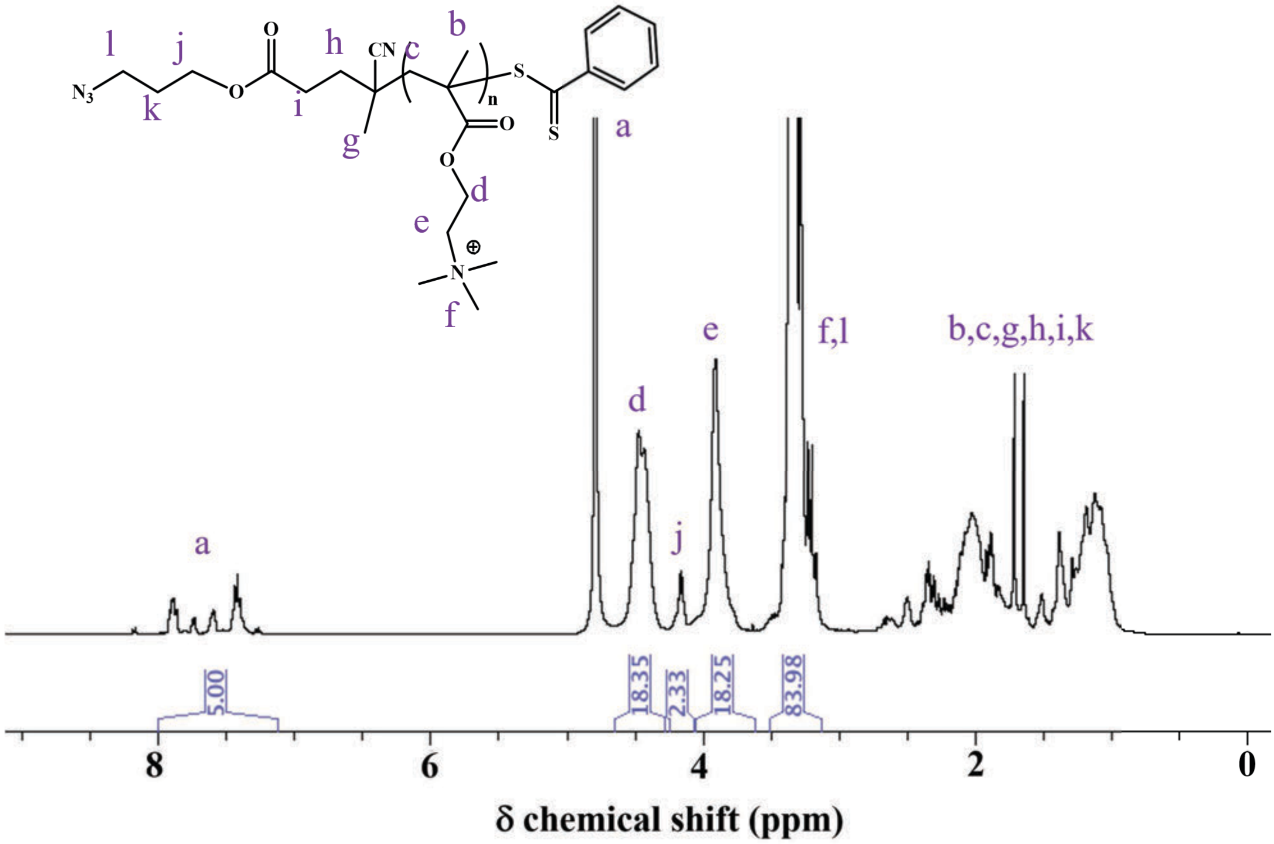

Figure S7. ^{1}H NMR spectrum P(TMAEMA)$_9$ in D_2O (25 °C, 400.2 MHz).

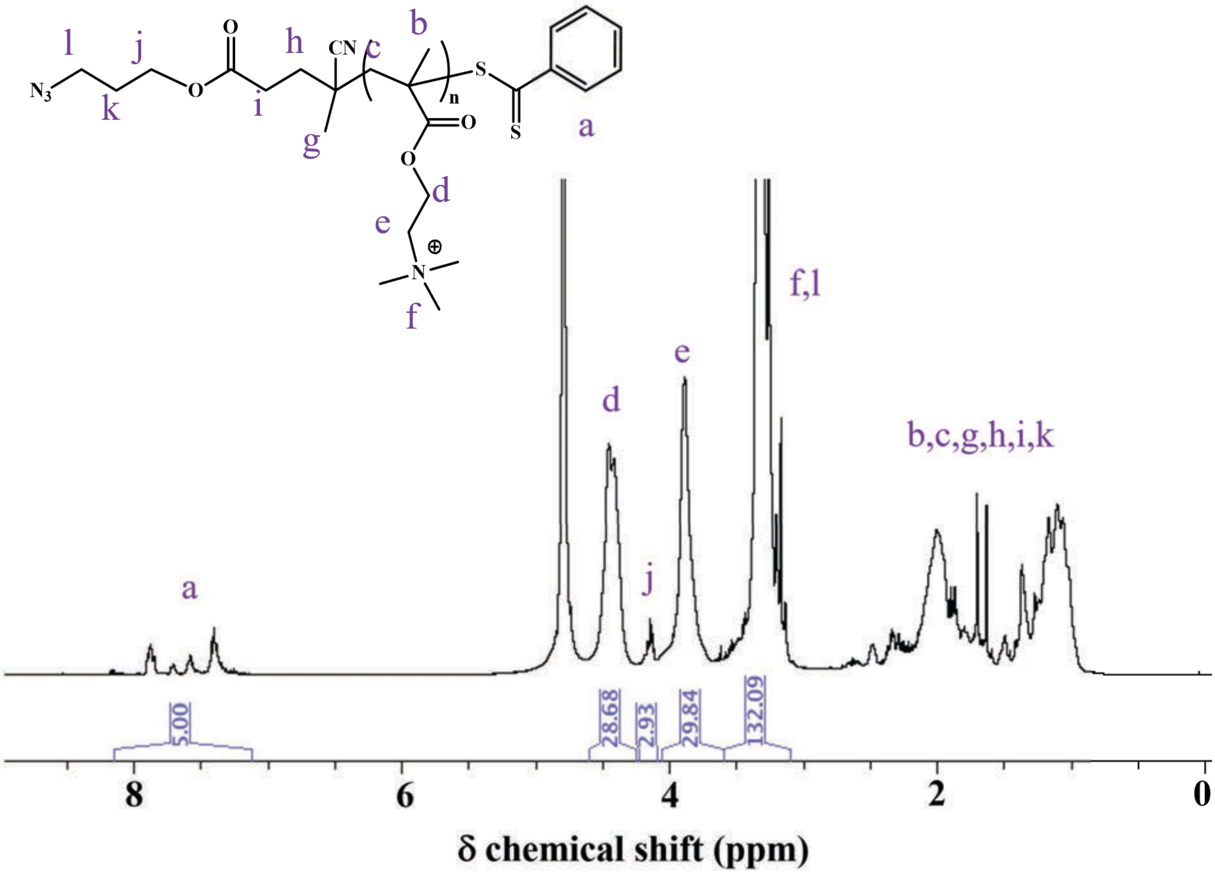

Figure S8. [1]H NMR spectrum in D_2O of P(TMAEMA)$_{15}$ in D_2O (25 °C, 400.2 MHz).

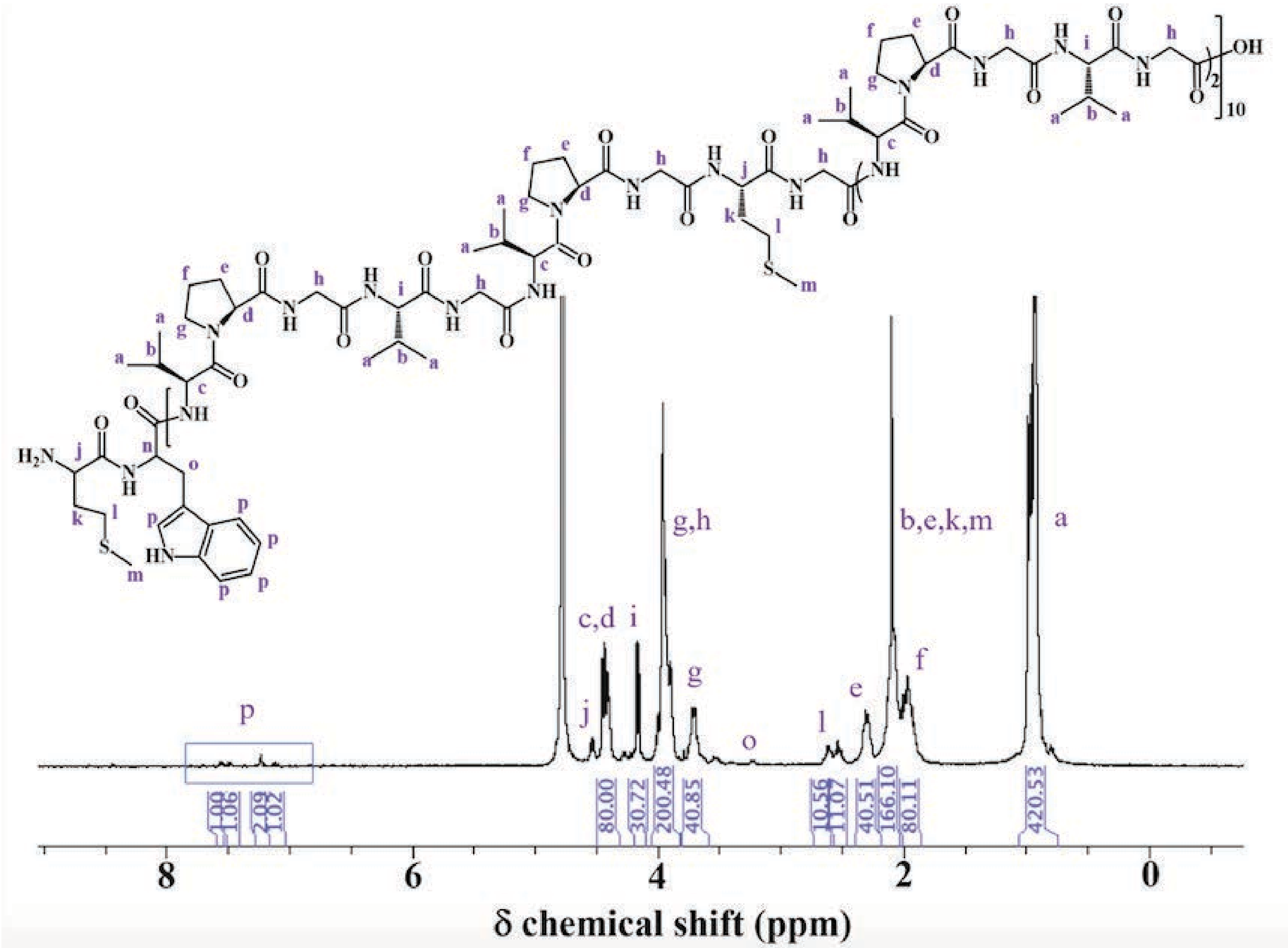

Figure S9.- ^{1}H-NMR spectra of ELP in D_2O (25 °C, 400.2 MHz).

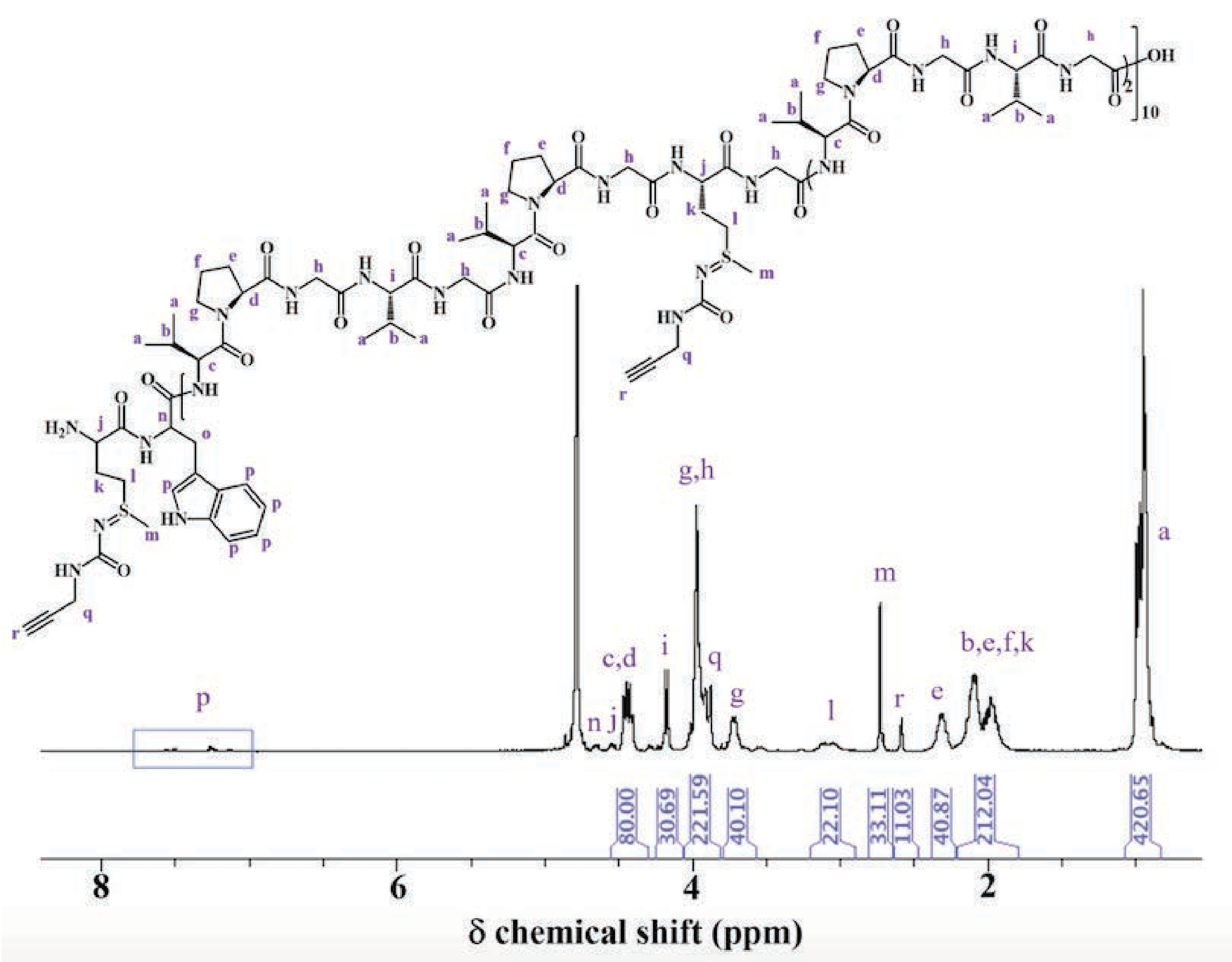

Figure S10.- ^{1}H-NMR spectra of alkyne-modified ELP in D_2O (25 °C, 400.2 MHz).

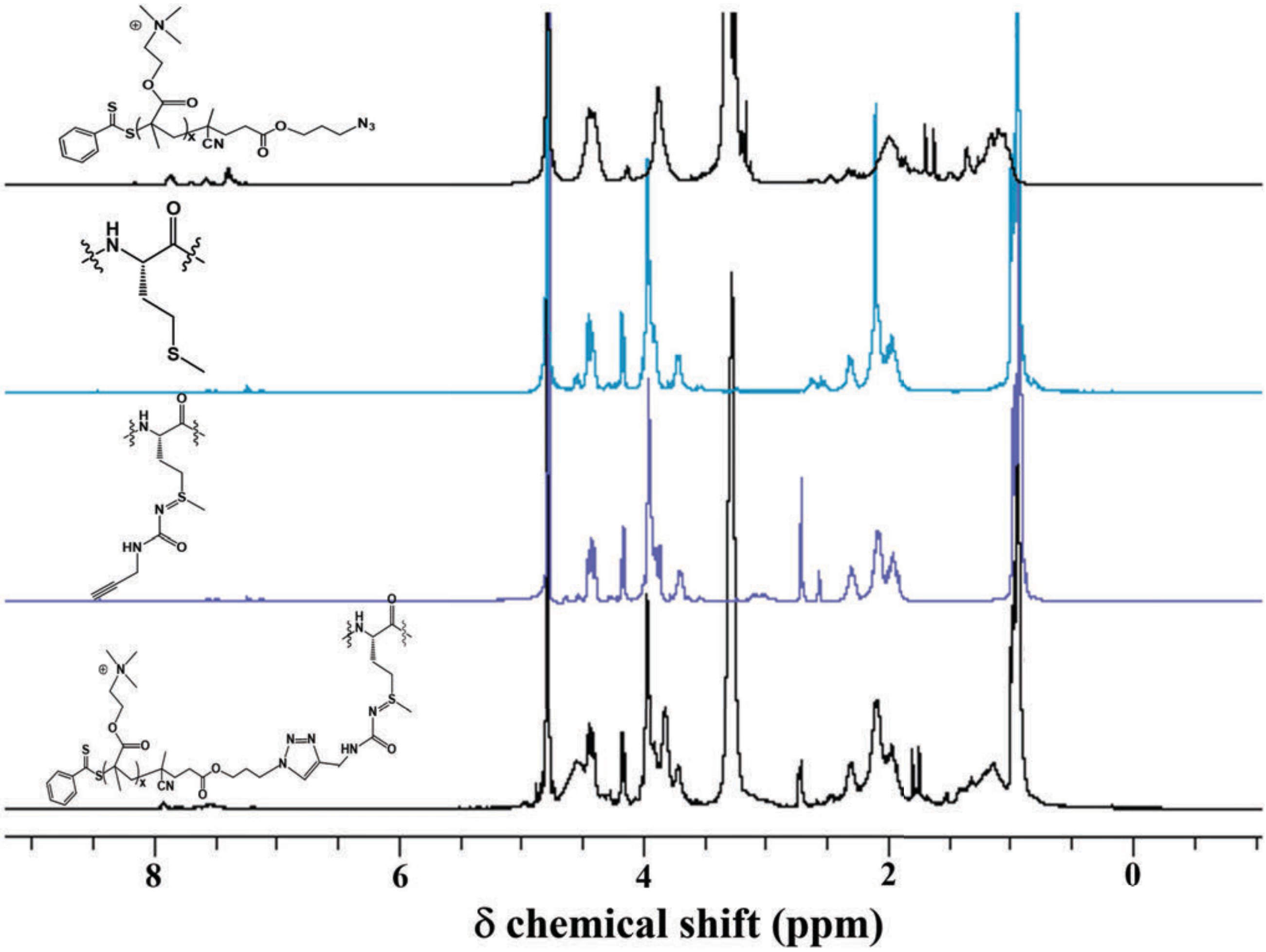

Figure S11. Superimposed ^{1}H NMR spectra of a) cationic oligomer P(TMAEMA)$_6$, b) ELP, c) ELP(alkyne) and d) ELP-g-P(TMAEMA)$_6$ in D_2O (25 °C, 400.2 MHz). Resonance # corresponds to *Val* αCH of the guest residue in VPGVG repeat units, and resonance corresponds to *Val* αCH and *Pro* αCH of VPGXG repeats.

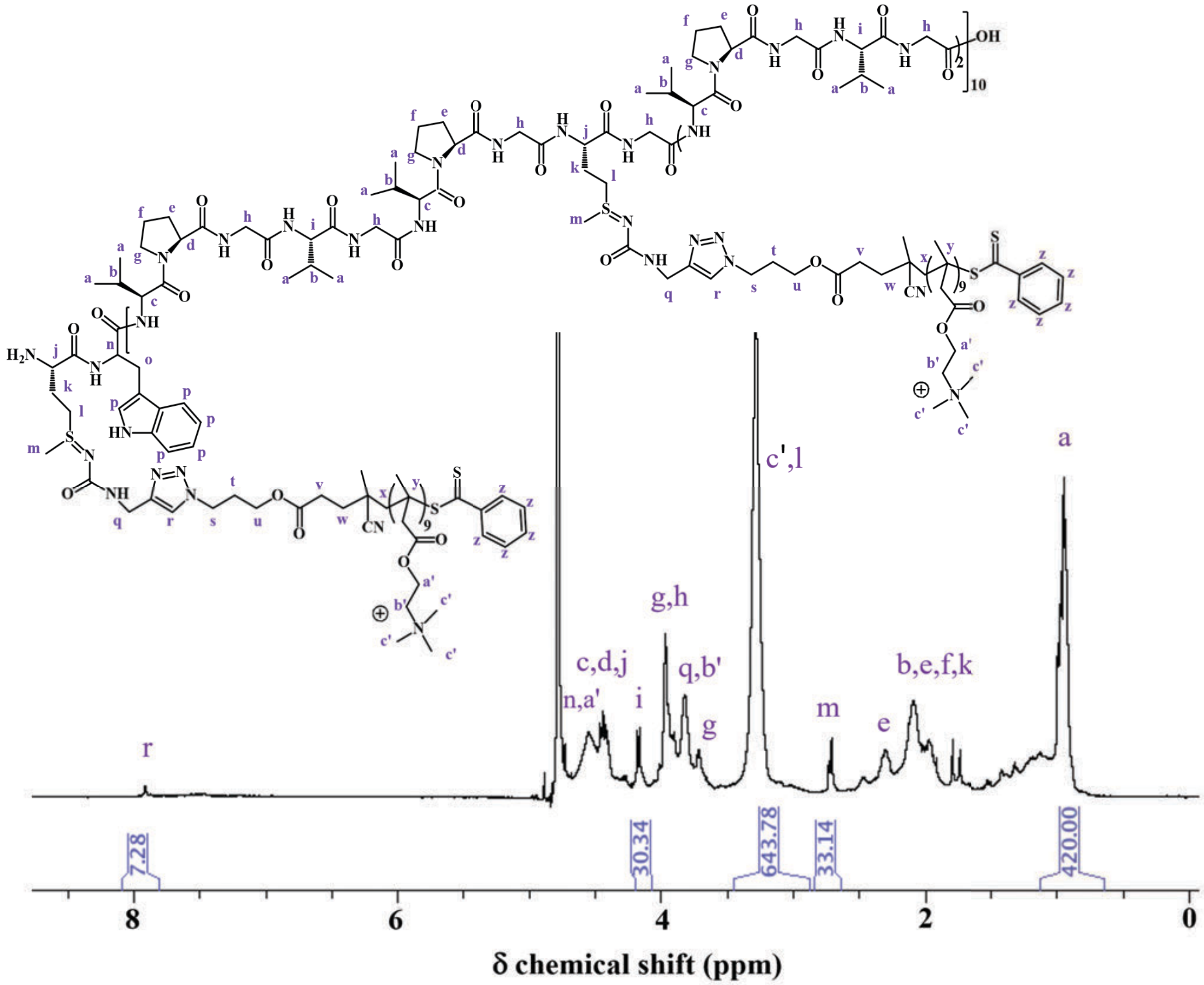

Figure S12.- [1]H-NMR spectra of ELP-*g*-P(TMAEMA)$_9$ in D_2O (25 °C, 400.2 MHz).

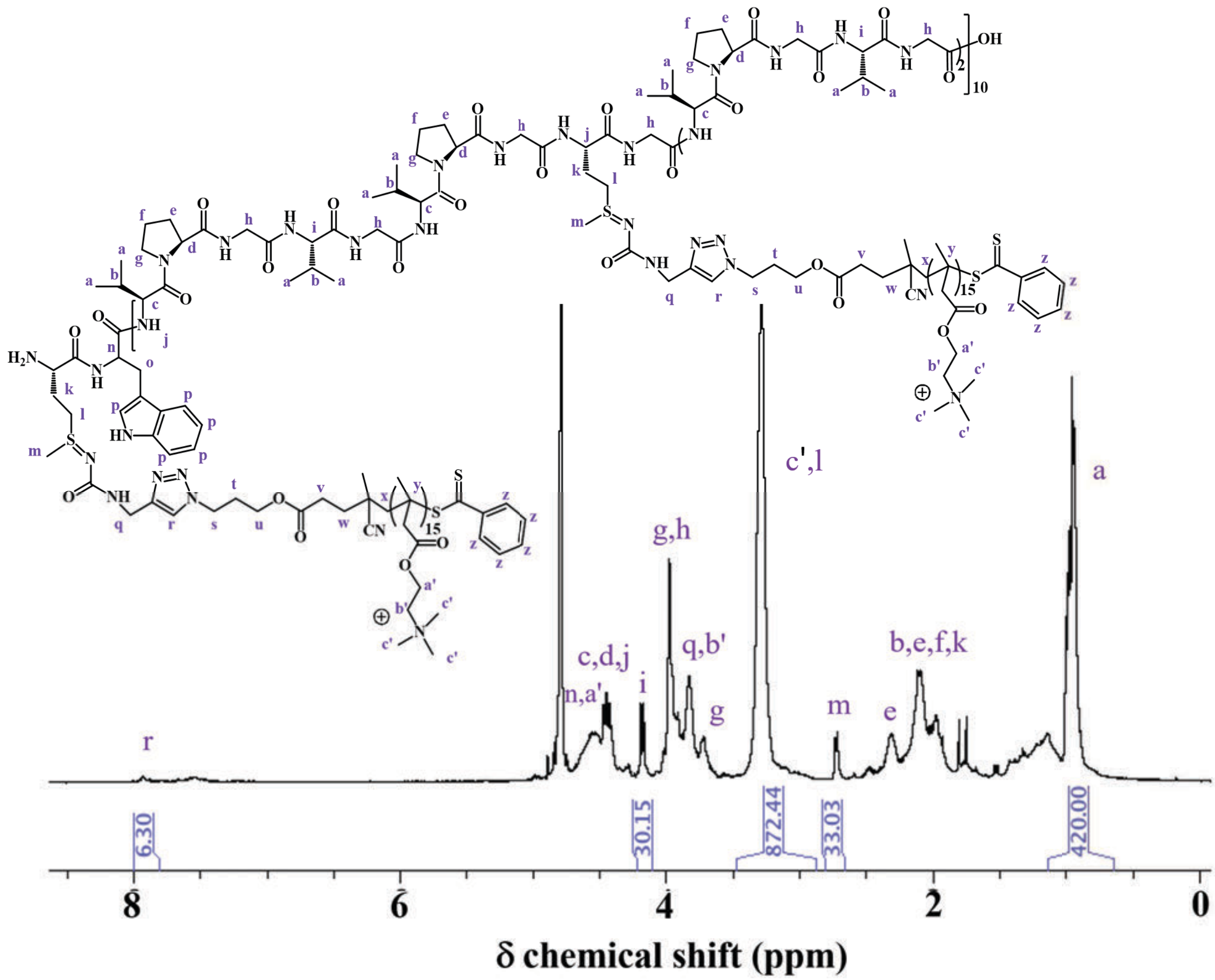

Figure S13.- ^{1}H-NMR spectra of ELP-*g*-P(TMAEMA)$_{15}$ in D_2O (25 °C, 400.2 MHz).

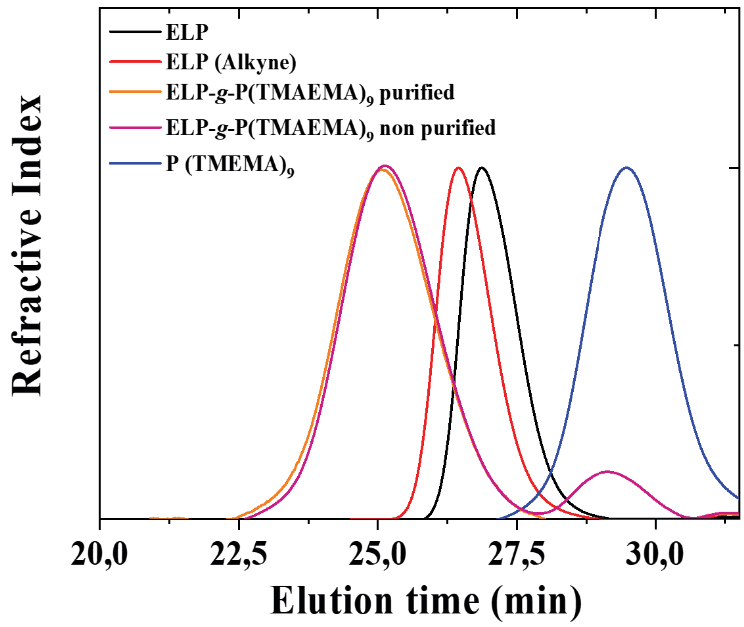

Figure S14.- SEC traces in AcOH/Ammonium Acetate/ACN of ELP (black), ELP(Alkyne) (red), ELP-*g*-P(TMAEMA)$_9$ purified (orange), ELP-*g*-P(TMAEMA)$_9$ non purified (pink) and P(TMAEMA)$_9$ (blue) using a RI detector.

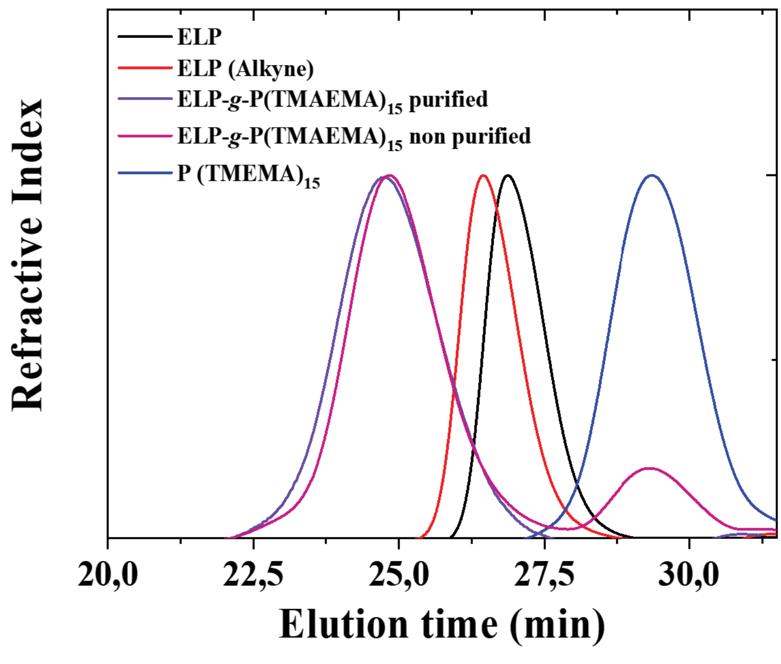

Figure S15.- SEC traces in AcOH/Ammonium Acetate/ACN of ELP (black), ELP(Alkyne) (red), ELP-*g*-P(TMAEMA)$_{15}$ purified (purple), ELP-*g*-P(TMAEMA)$_{15}$ non purified (pink) and P(TMAEMA)$_{15}$ (blue) using a RI detector.

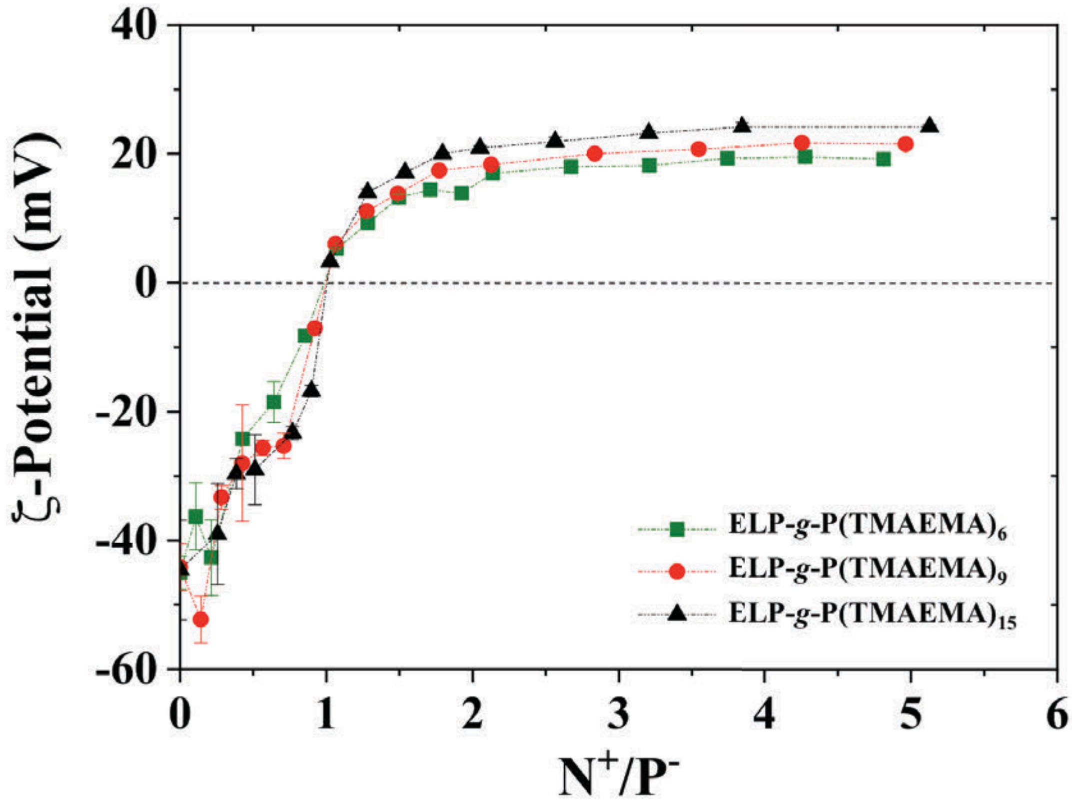

Figure S16.- ζ-potential as a function of N^+/P^- ratio during ELP-*g*-P(TMAEMA)$_X$ complex formation. Conventional slow dropwise mixing of ELP-*g*-P(TMAEMA)$_X$ to a pDNA solution was used for these measurements. Temperature measurement: 37 ºC. C_{pDNA} = 0.005 mg/mL prepared in Tris 10 mM buffer at a pH=7.4, $C_{ELP\text{-}P(PTMAEMA)6,9\ or15}$= 0.2 g/L prepared in water at pH = 6.0.

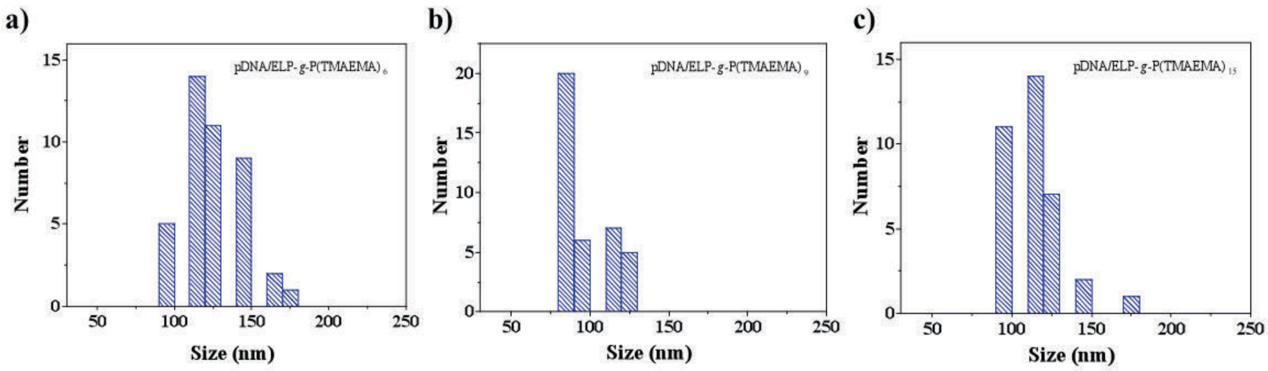

Figure S17.- Particle size distribution from AFM measurements for a) pDNA/ELP-*g*-P(TMAEMA)$_6$, b) pDNA /ELP-*g*-P(TMAEMA)$_9$ and pDNA /ELP-*g*-P(TMAEMA)$_{15}$ complexes prepared at the charge ratios N^+/P^-=10. C_{pDNA}= 0.03 mg/mL prepared in Tris 10 mM buffer at a pH=7.4 $C_{ELP\text{-}P(PTMAEMA)6,\ 9\ or15}$= 0.2 mg/mL prepared in water at pH = 6.0.

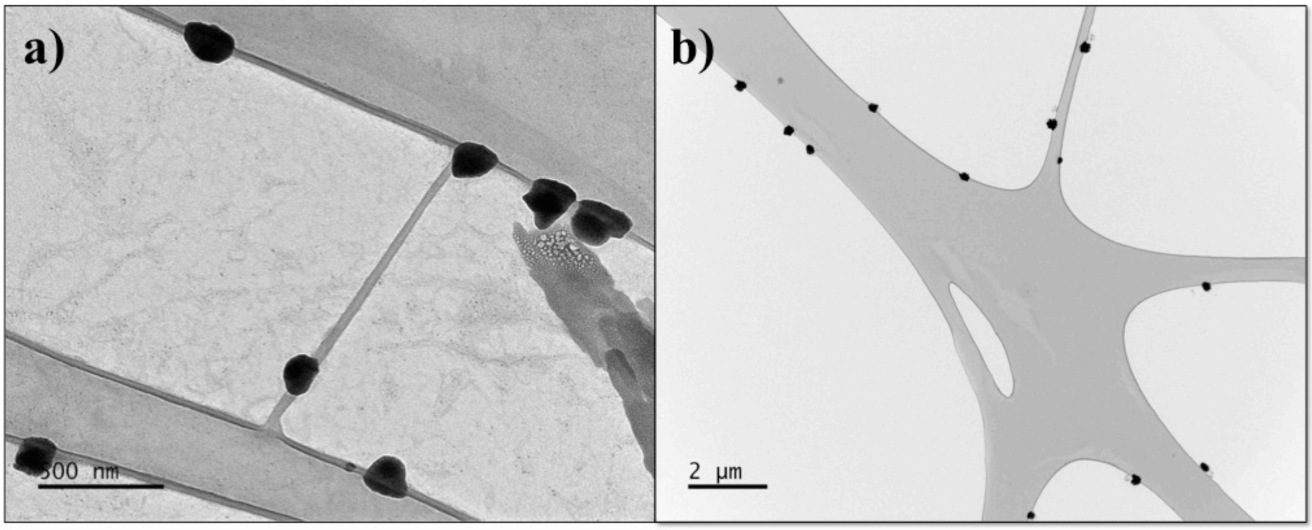

Figure S18.- TEM images of a) pDNA/ELP-*g*-P(TMAEMEA)$_6$ and b) pDNA/ELP-*g*-P(TMAEMEA)$_9$, prepared at a charge ratio N^+/P^- =10. C_{pDNA} = 0.03 mg/mL prepared in Tris 10 mM buffer at a pH=7.4, $C_{ELP\text{-}P(PTMAEMA)6,9\ or15}$= 0.2 g/L prepared in water at pH = 6.0.

Internet link

https://www.dropbox.com/s/9ofjg94i9pruqg1/2-A1-48h.avi?dl=0

Video S1.- Movie made from a 3D reconstruction of a typical cell after 48 hours of post-transfection

References supporting information

[1] Quemener Damien; Davis Thomas P; Barner-Kowollik Christopher; Stenzel Martina H. *Chemical communications* (**2006**), (48), 5051-3.

[2] Ishii, Tsuyoshi; Okahata, Yoshio; Sato, Toshinori. *Chemistry Letters* (**2000**), (4), 386-387.